Solar Energy 304 (2026) 114174

Contents lists available at ScienceDirect

Solar Energy

journal homepage: www.elsevier.com/locate/solener

Characterization of an opaque ventilated façade applied to a living laboratory: A seasonal experimental thermal performance analysis under real conditions

Graziano Salvalai

Department of Architecture, Built Environment and Construction Engineering, Politecnico di Milano – Via Giuseppe, Ponzio 31, 20133 Milan, Italy

ARTICLE INFO

Handling editor: XXXX

Keywords:
Opaque ventilated façade
Dry-layer wall technology
Experimental measurements
Thermal and energy performance
Living laboratory
Temperature distribution

ABSTRACT

The present work focuses on a long-term, experimental monitoring analysis of an Opaque Ventilated Façade (OVF) system applied to a dry-assembled, wood-based wall technology. The real-scale prototype of the façade was installed in the full-scale facility developed under the MEZeroE, H2020 EU funded project. A detailed monitoring campaign has been conducted during summer and winter to assess the OVF performance under real operation. The experimental study allowed the characterization of the main OVF variables: i) temperature of the OVF layers, ii) air speed inside the cavity, iii) air temperature inside the cavity, iv) heat flux across the OVF and a reference non-ventilated façade, v) correlation between the different key variables. During summer days, the minimum and maximum cavity air speed is respectively 0.6 m/s and 1.2 m/s; during winter days the cavity air speed is stable and around 0.4–0.5 m/s. In summer the OVF shows a linear correlation between the air speed and the temperature of the air cavity ($R^2 = 0.76$) and between the air cavity and the external air temperature ($R^2 = 0.96$). From an energy efficiency perspective, the OVF contributes to a reduction in peak cooling loads by approximately 2.0–3.0 W/m^2 and peak heating loads by approximately 0.9–1.0 W/m^2. Architects and engineers can use the experimental results as a reliable scientific basis to design and accurately predict the performance of similar façade systems.

1. Introduction

Lowering CO_2 emissions and energy demand are fundamental goals set by the European Commission Green Deal towards a carbon neutral continent [1]. With more than half of European residential buildings built before the first thermal regulations entry into force in 1970 [2], the construction sector is critical for meeting these targets. Therefore, the EU has promoted a long-term renovation strategy to double the annual energy renovation rate of residential and non-residential buildings by 2030 [3]. The strategy consists of promoting deep retrofits of the existing buildings to achieve zero carbon performance levels by 2050, as required by the latest Energy Performance of Buildings Directive (EPBD) recast [4]. A detailed analysis of the building envelope is the first step toward lowering heating and cooling energy consumptions. The design of the building envelope is essential for establishing the serving demand for thermal comfort, as well as ensuring comfort, indoor air quality and safety. Its layout is also important to determine its carbon footprint [5]. The envelope serves as a barrier to the outdoor, reducing heat gains and losses, and it is the primary passive regulator of internal conditions. External Thermal Insulation Composite System (ETICS) is one of the most widely used building envelope retrofit system. It consists of an insulating shell applied to the external façades of the building to reduce thermal transmittance and consequently ensure energy and cost saving goals. However, in recent years, architects have shown a special interest in the integration of Opaque Ventilated Façades (OVFs) in a variety of building typologies, climates, and geometrical configurations [6]. This technology, widely adopted in new constructions and renovation projects for both residential and non-residential buildings, is characterized by the presence of an external cladding anchored to the wall surface through a typical aluminium frame and separated from the thermal insulation layer by a ventilated air gap. The cladding protects the façade against external influences such as solar radiation, water, and mechanical stress, and can be composed of many materials such as stone, ceramic, clay, brick, wood-based panels, precast concrete, metal, composite, and also photovoltaic panels [7,8,9]. Ventilated façades, although not extensively analysed like Double Skin Facades (DSFs), have proven to be an effective passive solution for reducing the cooling needs mainly in warm climates [10], thanks to the dissipation of accumulated heat promoted by convection in the air cavity and shading of the

E-mail address: graziano.salvalai@polimi.it.

https://doi.org/10.1016/j.solener.2025.114174
Received 27 August 2025; Received in revised form 2 November 2025; Accepted 17 November 2025
Available online 24 November 2025

Nomenclature

AC_vent	Air capacity inside the cavity [m^3/h]
OUF	Opaque Unventilated Façade
OVF	Opaque Ventilated Façade
PDF	Probability Density Function [%]
RAD_amb	Solar radiation on vertical surface [W/m^2]
HF_{UF}	Heat flux unventilated façade [W/m^2]
HF_{VF}	Heat flux ventilated façade [W/m^2]
RH_amb_{ext}	External ambient relative humidity [%]
RH_vent	Relative humidity inside the cavity [%]
T_amb_{ext}	External ambient temperature [°C]
T_sup_{ext}	External surface temperature [°C]
T_amb_{int}	Internal ambient temperature [°C]
T_sup_{int}	Internal surface temperature [°C]
T_clad_{HF}	Cladding surface temperature – high front [°C]
T_clad_{LF}	Cladding surface temperature – low front [°C]
T_clad_{B}	Cladding surface temperature – back [°C]
T_glass_{HF}	Fiberglass surface temperature – high front [°C]
T_glass_{LF}	Fiberglass surface temperature – low front [°C]
T_glass_{HB}	Fiberglass surface temperature – high back [°C]
T_glass_{LB}	Fiberglass surface temperature – low back [°C]
T_vent	Air temperature inside the cavity [°C]
V_vent_{H}	Air speed inside the cavity – high [m/s]
V_vent_{L}	Air speed inside the cavity – low [m/s]

Fig. 1. Weather station installed nearby the testing facility and equipped with: wind direction sensor (1), anemometer (2), globe temperature sensor (3), air temperature and relative humidity sensor (4), class A pyranometer (5).

cladding [11,12]. However, the overall performance of a ventilated façade, even under the same boundary conditions, can be affected by several parameters such as geometry, orientation, thermos-physical characteristics of the wall layers, thermal insulation thickness, air cavity thickness, cladding material and colour [13,14], presence and typology of the joints between the cladding elements [15], and air permeability of the perforated grill at the bottom of the ventilated cavity [16,17]. Massive external claddings with high thermal inertia, for example, can operate as thermal buffers between the outdoors and the air cavity, thereby reducing heat fluxes through the envelope in both summer and winter [18]. In the same way, smaller air cavities increase the air speed and flow reducing heat gains [19]. On the contrary, point thermal bridges generated by the cladding's anchoring system, if not solved with thermal pads on brackets and nail sealing tapes, can

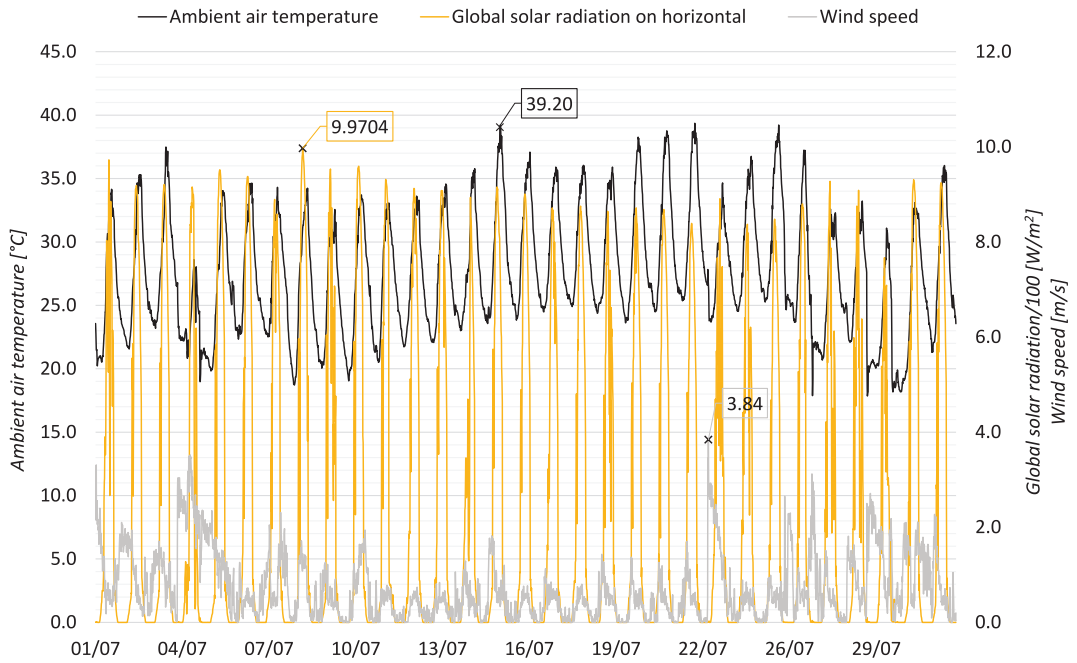

Fig. 2. Ambient air temperature, global solar radiation on horizontal surface and wind speed measured during July 2023.

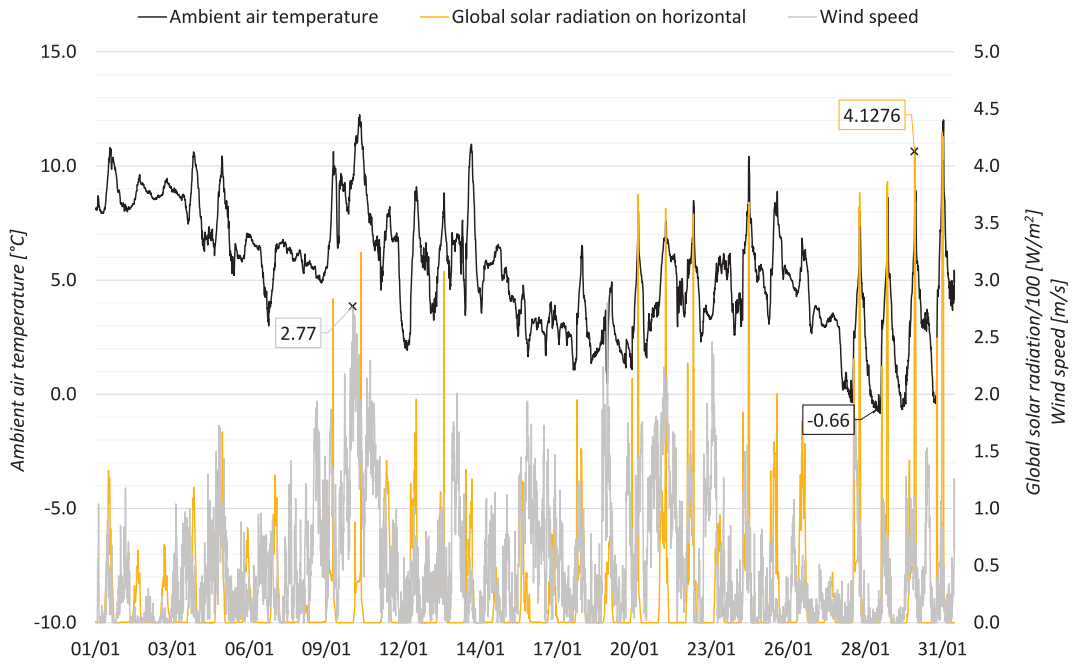

Fig. 3. Ambient air temperature, global solar radiation on horizontal surface and wind speed measured during January 2023.

negatively affect the efficiency of the ventilated façade, causing a difference between corrected and uncorrected thermal transmittance up to 70 % and an increase in heat losses up to 80 % [20,21].

Evaluating the performance of a ventilated façade, especially in comparison to a standard insulated wall, is challenging due to the limited availability of standardized software and data required to accurately assess the complex heat transfer mechanism occurring inside the air cavity, which can vary with changing weather conditions [22,23]. Weather conditions, in fact, play a critical role in determining the performance of ventilated façades, particularly of those designed to promote natural ventilation and dynamic thermal regulation. Factors such as wind speed and direction directly influence the pressure differentials across the façade governing the airflow rate and pattern inside the ventilated cavity. Similarly, fluctuations in ambient temperature affect the buoyancy-driven stack effect between the lower and the upper façade openings, either enhancing or inhibiting natural ventilation [24,25]. Finally, solar radiation contributes to heat gains on the external cladding, impacting the temperature gradient between the cavity and the interior wall surface [26]. These interactions all make ventilated façade systems inherently sensitive to external climatic conditions, with consequent significant variations in thermal performance, energy efficiency, and indoor comfort across different seasons and geographic locations.

Different approaches are used to evaluate OVFs energy performance,

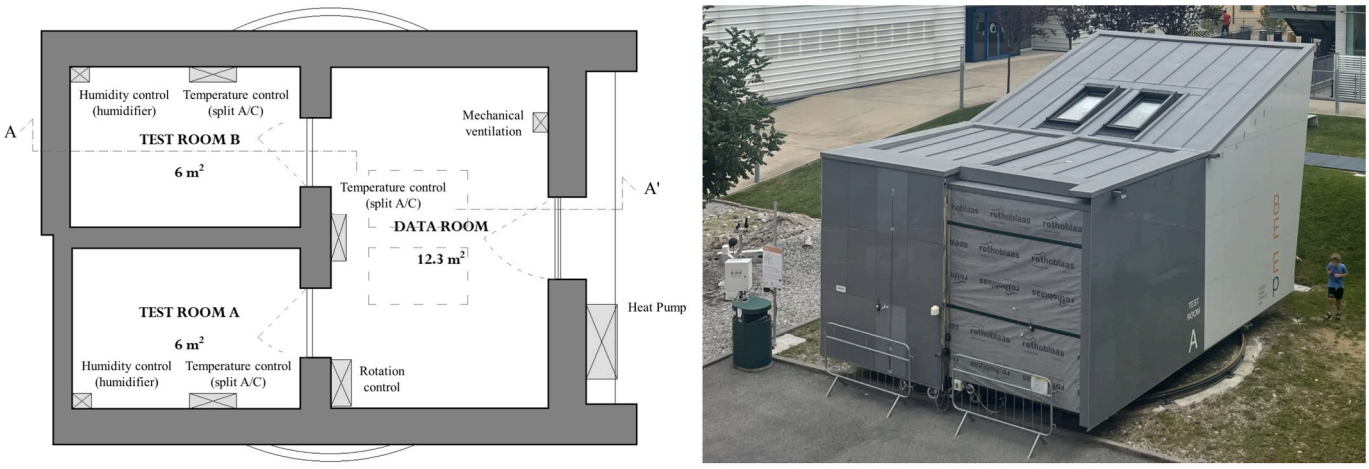

Fig. 4. Schematic representation of the laboratory concept (a) and view of the completed facility (b).

including numerical modelling, such as CFD, and experimental campaign. Several studies conducted detailed numerical [27,28] or computational fluid dynamic analyses [29] requiring high simulation skills and validated the results through available experimental data [24,30,31]. However, the results show large discrepancies between the numerical and the experimental evaluations, demonstrating the difficulty in predicting the performance of the OVF. Case studies therefore represent a valid solution to depict the behaviour of these systems under real weather conditions [32,33]. An experimental campaign conducted in a cold climate of China, for example, shows an energy use reduction for summer and winter of respectively 11.4 % and 6.5 % compared to a conventional unventilated façade [34], while a prototype of multilayer ventilated technology presents higher energy performance than conventional façades, with a reduction of thermal transmittance close to 30 % along the air cavity [35].

Based on the literature review of recent studies, the present work starts from the following considerations:

- The OVF received less attention than other wall configurations, such as Double Skin Façades [22,23,36,37,38,39,40].
- Most of the studies on OVF do not provide experimental analysis on real operational conditions, they mainly rely on simulation and numerical analysis [10,11,24,25,26,27,28,29,30,41,42].
- The airflow assessment behind ventilated wall assemblies is still lacking [43].
- Few studies have investigated the OVF performance in a humid subtropical continental climate such as the one representing Lombardy climate conditions, characterized by marked differences between hot and humid summers and cold and humid winters [31,44].
- Several studies on the thermal behaviour of OVF focus on summer season only, while limited analysis is carried out for winter configurations [13,17,18,25,26,30,34,44,45].
- The effects of some design features have not yet been deeply investigated experimentally, especially for open joint OVF with lightweight external finishing and dry-assembly wall layer construction [34,44].

The experimental activities were performed in the BEE Lab (Building façadE performancE Lab) outdoor test facility, located at Politecnico di Milano, Lecco campus, Italy, through a long-term monitoring campaign designed to detail the OVF temperature profile and the heat flux intensity under real, local climatic forces. This study is distinguished by the use of a dedicated full-scale testing set-up which enables the comprehensive evaluation of façade performance under controlled yet realistic environmental conditions and across different orientations. A key novelty of this work lies in the generation of experimental data on a real-scale ventilated façade, a level of detail rarely addressed in current literature. Furthermore, the adoption of an acrylic-based cladding material introduces an innovative approach in the field, where ventilated façades are traditionally constructed using heavier materials such as stone or porcelain tiles. The use of acrylic offers a lightweight, durable, and potentially more sustainable alternative, broadening the possibilities for façade design and application. The present research activity thus contributes in: i) experimentally verify the temperature distribution of the different OVF layers during hot summer and cold winter days, ii) report the correlation between the temperature level of the façade and the air velocity of the OVF cavity in hot and cold seasons, iii) prove the buoyancy effect in a typical OFV layout under different weather conditions. This study also provides effective insights on OVFs to professionals and construction companies, as well as data to researchers for validating numerical models of similar solutions.

The present paper is structured as follows: Section 2 provides an overview of the experimental set-up, focusing first on the lab infrastructure and then on the wall technology under investigation. The section also presents a detailed overview of the employed sensors' technology and positioning. The results of the long-term monitoring campaign are instead presented in Section 3, which is dedicated to the actual strategies implemented in the design and development phase of the building. Finally, Section 4 reports the main findings and conclusions.

2. Methodology

This paper presents in detail the results of the long-term experimental activities carried out on an OVF characterized by an innovative, thin (8 mm), acrylic-based, solid-surface cladding. The 12-months monitoring has been carried out in 2023 in the experimental Building façadE performancE Lab living laboratory, a full-scale test facility located in Lecco, inside the university campus of Politecnico di Milano. Lecco (45°51′ N, 9°24′ E, 214 m ASL) is a typical temperate-climate city lying at the end of the south-eastern branch of Lake Como, 45 km far from Milan, and surrounded by mountains. According to Köppen-Geiger classification, the location falls within Cfb climate zone, but the presence of the lake locally exerts a mitigating influence [46]. For this reason, a dedicated weather station was installed nearby the lab (Fig. 1) to characterize the typical summer and winter local conditions under which the testing activities have been carried out.

Fig. 2 presents a time series comparison between ambient air

Fig. 5. Pictures of BEE Lab construction phases: rotating steel platform installation (a), prefabricated wood-based envelope assembly (b), ventilated facade installation (c), completed lab (d).

temperature (in °C), global solar radiation on horizontal surface (in W/m^2) and wind speed (in m/s) during July 2023, effectively illustrating how solar radiation acted as the primary driver of daily temperature variations. July registered the highest average temperature, while the typical maximum temperature ranged between 32 °C and 35 °C, with peaks of 39 °C. The solar radiation, instead, reached peaks of almost 1000 W/m^2 during the central hour of the day.

Fig. 3 displays instead the trend of ambient air temperature, global solar radiation on horizontal surface and wind speed during January 2023, Lecco's coldest month in which a notable temperature drop occurred together with limited daily variation. In this period, the minimum recorded temperature was −0.66 °C, while the maximum one reached 12.2 °C. During sunny days, the solar radiation overcame the threshold of 300 W/m^2, with peaks of 420 W/m^2.

2.1. Full-scale innovative test facility

The BEE Lab facility has been designed for testing new dry-assembly building envelope components and technologies for Zero Energy Buildings under real environmental and use conditions as part of the European H2020 founded project MEZeroE (Measuring Envelope systems for Zero Energy buildings) [47], which aims at implementing a European Open Innovation ecosystem [48] to: i) foster the development of nZEB envelope solutions, ii) transfer knowledge from research to the market, iii) match testing needs with existing facilities, iv) monitor living labs, v) standardize cutting-edge building envelope solutions. From the architectural point of view, the research facility is divided in two separate areas: two test rooms, characterized by a plug and play system facilitating the mounting and dismounting of walls and roofs samples (Fig. 4a), and a data room working space, where researchers analyse and discuss the monitoring outputs. BEE Lab is therefore a fully functional and operative testbed allowing to assess different multilayer

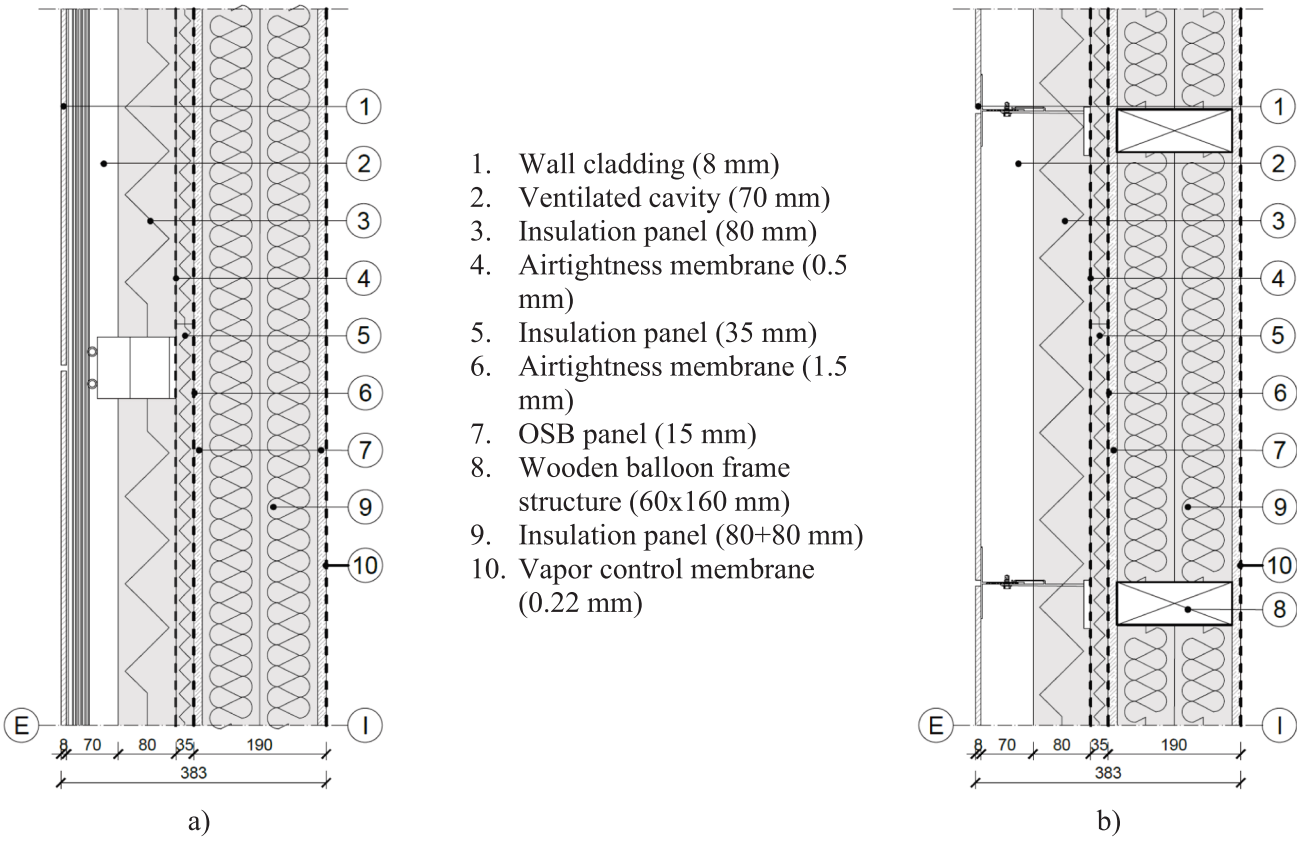

Fig. 6. A) vertical section of the ovf with the description of the layer composition; b) horizontal section of the ovf with the description of the layer composition.

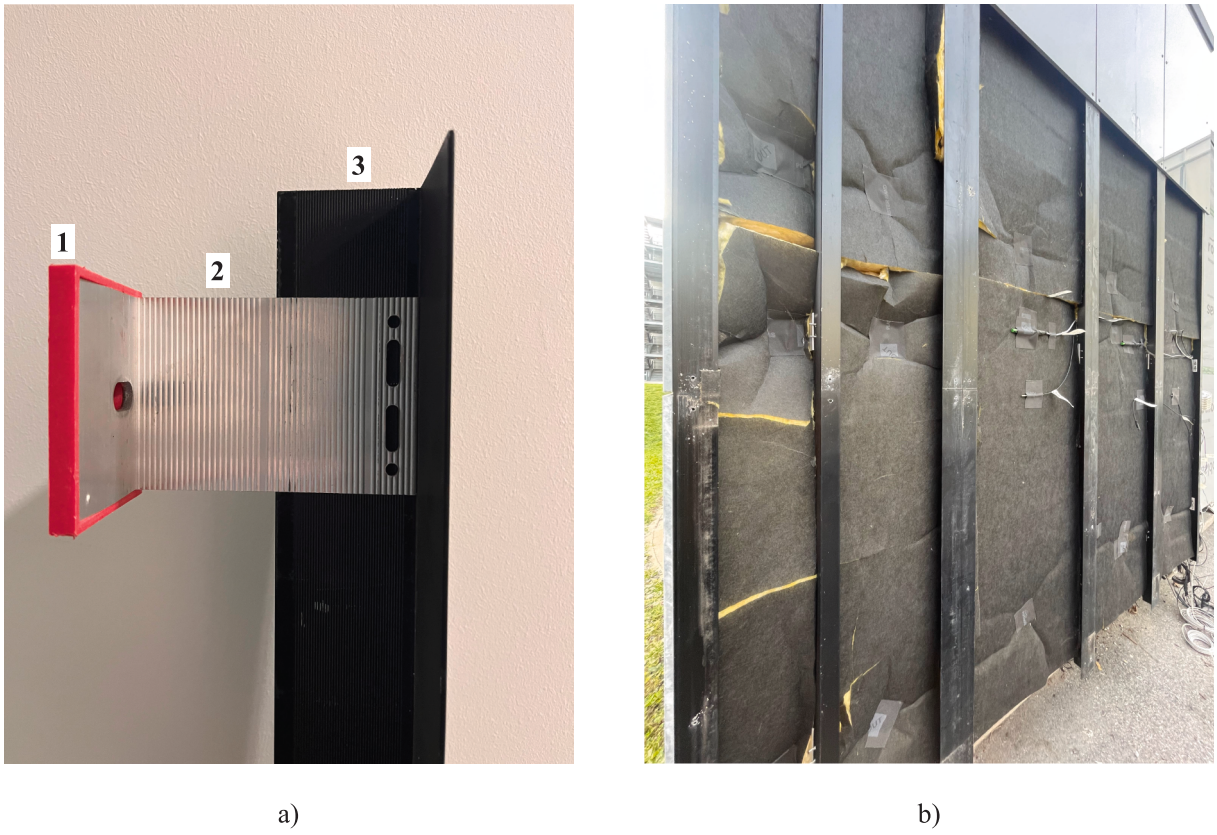

Fig. 7. A) ovf mounting system: 1) polypropylene thermal pad, 2) horizontal aluminium bracket (length 120 mm, width 68 mm, height 86 mm), 3) T-shaped rail for vertical installation (height 60 mm, width 120 mm); b) OVF installed on BEE Lab.

Table 1
Manufacturer thermo-physical characteristics of the walls under investigation. From left to right: layer number, material name, thickness [m], material conductivity λ [W /(m K)], material density ρ [kg/ m^3] and material heat capacity Cp [J/(kg K)].

Layer	Material	Thickness [mm]	Conductivity − λ [W/(m K)]	Density − ρ [kg/ m^3]	Specific heat − Cp [J/(kg K)]
1	External wall cladding	8.0	0.231	1800	1360
2	Ventilated cavity	70.0	–	–	1005–1030
3	Insulation panel (glass wool)	80.0	0.032	30	1030
4	Airtightness membrane	1.0	0.400	360	1800
5	Insulation panel (wood wool)	35.0	0.065	400	1810
6	Airtightness membrane	1.5	0.170	1250	160
7	OSB panel	15.0	0.130	600	1000
8	Wooden balloon frame structure	160.0	0.150	550	1700
9	Rockwool insulation panel	160.0	0.039	120	1030
10	Vapor control membrane	0.22	0.200	400	1700

envelope solutions under real conditions (Fig. 4b).

What makes it rather innovative for the field, especially in the Italian context, is the possibility to accurately test and monitor such technologies under actual operation conditions and in variable orientations. The testing area has been studied to have two adjacent identical test rooms ("Test Room A" and "Test Room B") for the simultaneous evaluation of different envelope solutions. A double chamber set-up, in fact, can be useful for experimental control purposes, as well as to conduct simultaneous measurements that would otherwise be disturbed by differences in boundary conditions. The two test rooms are both equipped with an air conditioning split for temperature control connected to an external heat pump (EER = 4.48, COP = 4.79, heating capacity = 6.80 kW, cooling capacity = 5.20 kW) and a manual humidifier able to spray about 500 g/h of water (electric absorbed power = 40 W, service temperature range = 1–40 °C, relative humidity range = 0–95 %). The "Data Room" of the laboratory is instead dedicated to the assessment of different envelope solutions under actual operation conditions, thanks to the involvement of the specifically designed and sensorized office environment occupants. This space aims, in fact, to not only monitor the building enclosure in real conditions, but also to study the effect of different solutions in terms of users' comfort and thermal perception. For this reason, the control parameters of temperature, relative humidity, air flow, and natural/artificial lighting are made available to the occupants. Another peculiarity of the facility is the full rotability of the testbed on dedicated motorized, circular tracks to accommodate different orientations according to test and research needs (Fig. 5a).

From a technological point of view, the whole structure is made of prefabricated dry-assembly wood components (Fig. 5b) with insulated cavities (λ = 0.065 W/mK), vapor barrier, airtightness and waterproofing membranes in order to fully characterize this technology in terms of performance over time and durability. The wood wool insulation thickness varies based on the envelope technological component, from a minimum of 35 mm in the test rooms roof and party wall to a maximum of 160 mm in the floor. The OVF cladding is instead composed of acrylic, solid-surface panels mounted on a vertical aluminium structure (Fig. 5c and d). More detailed information about the thermos-physical characteristics of the employed materials can be found in

Fig. 8. Front view of the living laboratory, on the left side the monitored OVF and on the right side the wall without the OVF technology;

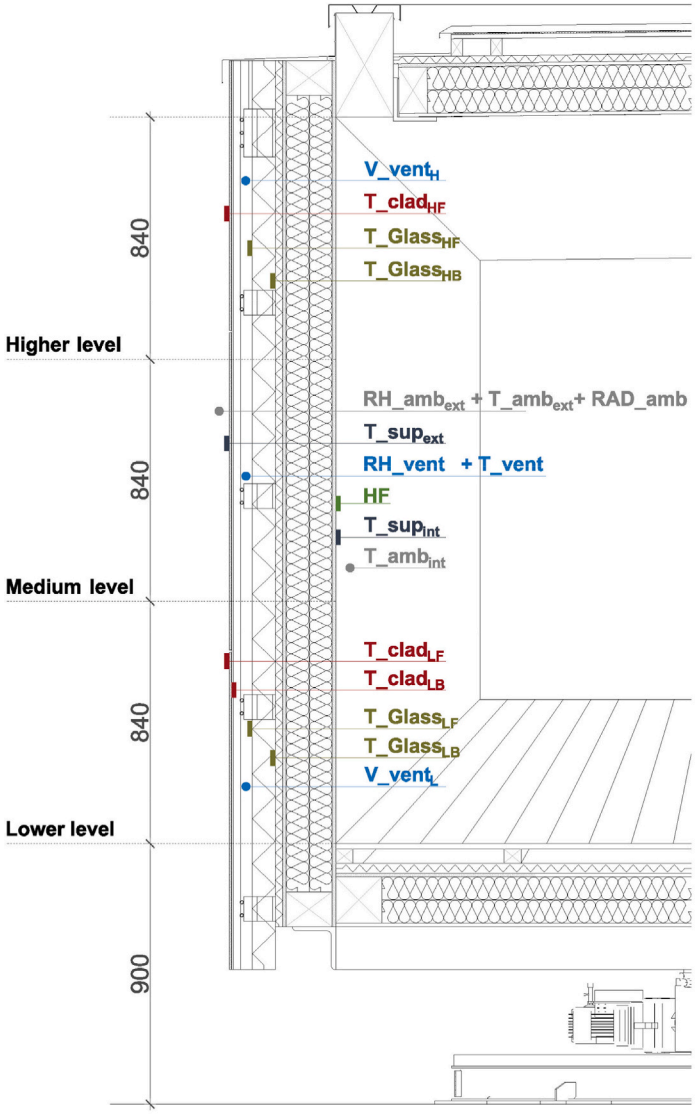

	Variable	Description and metrics
Higher level ~ 2,2-3,0 m	V_vent_H	Air velocity in the façade cavity – high [°C]
	T_cald_{HF}	Cladding surface temperature – high front [°C]
	T_glass_{HF}	Fiber glass surface temperature – high front [°C]
	T_glass_{HB}	Fiber glass surface temperature – high back [°C]
Medium level ~1,3-2,2 m	RH_amb_{ext}	External ambient relative humidity [%]
	T_amb_{ext}	External ambient temperature [°C]
	RAD_amb	Ambient solar radiation [W/m^2]
	T_sup_{ext}	External surface temperature [°C]
	RH_vent	Relative humidity in the façade cavity [%]
	T_vent	Air temperature in the façade cavity [°C]
	HF	Heat flux [W/m^2]
	T_sup_{int}	Internal surface temperature [°C]
	T_amb_{int}	Internal air temperature [°C]
Lower level ~ 1,3 m	T_clad_{LF}	Cladding surface temperature – low front [°C]
	T_clad_{B}	Cladding surface temperature – back [°C]
	T_glass_{LF}	Fiber glass insulation surface temperature – low front [°C]
	T_glass_{LF}	Fiber glass insulation surface temperature – low front [°C]
	V_vent_L	Air velocity in the façade cavity – low [m/s]

Fig. 9. Infographic depicting the OVF vertical section (left) outlining the position and codes of the sensors. The right part of the picture detail the sensor codes and the corresponding recorded parameters, categorized by their position along the façade.

Section 2.2.

2.2. *Opaque ventilated façade design*

The façade under investigation, which geometry (number of layers, cavity thickness, type of insulation, anchoring system, etc.) can be considered as a representative OVF construction solution, is characterized by a surface area of 8.75 m^2 and it is equipped with a set of sensors for the complete characterization of the ventilative cavity and the temperature profile of the different wall's layer. The façade is finished with a cladding system composed by an acrylic-based solid surface material [49] with variable dimensions (in line with the geometric and structural profile of the building), with RAL colour 7037 (dusty gray). The investigated ventilated façade system is a commercial type, featuring aluminium standard vertical rails and brackets. The geometry of brackets and rails was selected to assemble a ventilated façade system that complies with energy efficiency standards for typical vertical external walls across the different climate zones of Italy (Fig. 6). The cladding type was selected by the producer, who requested specific testing to verify its behaviour and efficiency under real operating conditions.

The present work presents and discuss the long-term monitoring study of the opaque ventilate façade finished by novel cladding panels made of an innovative acrylic-based solid surface material. Solid surface is a manufactured material that was most frequently used in design home furniture, where non-porosity and ease of maintenance are highly valued and prioritized. This material has been more recently applied for the same qualities also in architecture as a cladding in rain screen façades, exploiting its properties of durability, cleanability, low moisture absorption with high resistance to stains, environmental pollutants, detergents, humidity and freeze–thaw conditions. The present paper reports the results of different mechanical and thermal tests conducted on a novel composite acrylic-based solid surface named Materica Surface. The material is made of Azanite®, based on acrylic resins, and it is available in sheets of various thicknesses/dimensions ideated for ventilated façades application [49]. Fig. 6 report the OVF vertical wall section indicating the material and the thickness. This multi-layered wall design integrates effective thermal insulation, controlled

Fig. 10. Indoor monitoring setup of the OVF: 1) temperature and relative humidity between wall/roof layers; 2) air temperature and relative humidity; 3) wall/roof heat flux and internal surface temperature; 4) air conditioning split for temperature control; 5) wall internal surface temperature; 6) data logger; 7) relative humidity level controller.

ventilation, airtightness, and moisture management within a sturdy wooden frame (Fig. 7). The ventilated cavity and multiple membranes work together to protect against moisture and air infiltration, ensuring energy efficiency and long-term durability. The detailed properties of the wall materials has been reported in Table 1.

Fig. 8 shows a front view of the Building façadE performancE Lab (BEE Lab) outdoor test cell at Politecnico di Milano. The structure on the left side features a ventilated façade, fully clad with smooth grey panels. This ventilated system includes an air gap behind the cladding, promoting airflow to enhance moisture control and thermal regulation. The right side represents the same structural technology but without the cladding installed, exposing the underlying weather-resistant membrane.

2.3. Monitoring equipment and sensors set-up

The sensors selection and placement strategy was developed following a comprehensive review of existing literature and grounded in the authors' domain expertise [24,32,45,49]. Specifically, two measurement points were established at distinct vertical locations, one near the base and the other at the top of the ventilated façade, to capture representative thermal and airflow dynamics. Although this approach imposes limitations due to the total height of the façade, it effectively targets the characterization of floor-to-floor behaviours. This is particularly relevant given that ventilated façades are typically segmented by intumescent cavity fire barriers, which serve as critical fire safety elements. The deliberate positioning of these sensors, combined with the overall sensor network configuration, facilitates the acquisition of essential data necessary for an accurate assessment of the ventilated façade's performance. The detailed sensors position is depicted in Figs. 9 and 10 reporting also the name of all the measured point for facilitating the readings of the monitoring results graphs.

The measurements were performed in accordance with UNI EN ISO 7726:2002 (Ergonomics of the thermal environment – Instruments for measuring physical quantities) [50] using sensors that were factory-calibrated by the manufacturers and accompanied by calibration certificates. Additionally, prior to installation, a cross-check calibration was conducted under controlled conditions to verify measurement consistency across identical sensor types. Periodic verification was also performed during the monitoring campaign to detect potential drifts or anomalies.

The OVF characterization has been carried out using the data logged by two separated measurement nodes, one located at the bottom of the OVF, at 1400 mm from the ground level and the second located at the top at 400 mm below the upper edge. Each measurement nodes has been composed by similar set of sensors: three surface temperature sensors plugged on the main wall layers and one air velocity sensor for outlining the air cavity behavior. For reaching a more accurate analysis the lower measurement point was integrated with an additional temperature sensor applied to the inner side of the OVF cladding panel. The heat flux and the air/humidity sensors (in the cavity) have been place, instead, at the middle of the wall. The air temperature and the vertical global solar radiation on the OVF have been measured respectively through a silicon pyranometer and a thermo-hygrometer with heat shield, the two sensors have been directly mounted on the OVF (Fig. 11e and f). The local weather conditions have been measured by a weather station located nearby the laboratory equipped with wind speed and wind direction, air temperature/humidity, globe temperature, solar global radiation on horizontal surface. All the variables have been collected with a data logging of 10 min, screening raw data to remove outliers and incomplete records due to power loss or sensor disconnection. A moving average filter has been applied to smooth high-frequency fluctuations while preserving underlying trend, with a window size based on the thermal time response of the façade system to avoid distortion of meaningful variations. The detailed technical characteristics of each sensor are collected in Table 2.

3. Monitoring results analysis

This section presents the results of the long-term monitoring study in terms of surface temperatures of the different OVF layers, air temperature and wind velocity of the ventilated cavity, as well as the heat fluxes

Fig. 11. Pictures of the sensors mounted on the OVF: a) surface temperature sensor on the external surface of the thermal insulation layer; b) air velocity sensor inside the OVF cavity; c) air temperature and air humidity sensor inside the OVF cavity; d) surface temperature sensor for the cladding temperature monitoring; e) global solar radiation sensor on the facade; f) air temperature at humidity sensor located 15 cm from the OVF and 1.5 m from the ground level.

through the ventilated cavity through the parameters that have been collected during both the summer and winter season. The summer performance analysis was conducted throughout July 2023, while the winter analysis was conducted in January 2023. These time periods were selected as they capture representative Lecco environmental conditions and façade performance under typical seasonal variations (Section 2).

3.1. Summer performance results analysis

This subsection describes the overall behavior of the OVF under summer conditions. Specifically, the characterization is based on a representative dataset collected between July 16th and 22nd, 2023. Throughout most of 2023, temperatures in Italy were above average, with the highest spike occurring in June, when temperatures exceeded long-term averages by 3.09°C. Fig. 12 summarises one week the temperature and solar vertical radiation trends in the various layers of the OVF technology. The global solar radiation measured on the façade reached peaks of 672 W/m^2, with a maximum air temperature of 40.03 °C. All the measured points of the OVF layer fluctuate accordingly to the solar energy intensity received. The temperature peak has been recorded on the external cladding surface reaching with a value of 61.94 °C. The maximum mean value over the whole period was equal to 59 °C.

During afternoon hours, when the façade is shaded, the outdoor cladding temperature drop immediately by 30–35 °C, reaching the same temperature of the ambient air. Fig. 12 illustrates the diurnal evolution of the ventilated cavity air temperature (*T_vent*), external ambient temperature (*T_amb,ext*), glass wool surface temperatures at different heights (HF, LF, HB, LB), and incident solar radiation on the vertical surface (*RAD_amb*) during the representative summer period (16–22

Table 2
List of the sensors and related characteristics.

Surface temperature sensor	Measure range	
Measurement range	−40 − +100°C	
Total accuracy	< ±0.2 °C from 0° to 50 °C	
Resolution	<0.03 °C from 0° to 50 °C	
Drift	<0.1 °C (0.18 °F) per year	
Air temperature/humidity sensor	**Measure range**	
Measurement range	T: −40 /+75°C	RH: 0–100 %
Total accuracy	T: ± 0.20°C	RH: ± 0.21 %
Resolution	T: 0.02°C	RH: 0.01 %
Drift	< 0.01 °C (0.18 °F) per year	< 1 % per year typical
Solar Radiation (Silicon Pyranometer)	**Measure range**	
Measurement range	0–1280 W/m^2	
Operating temperature range	−40° to 75 °C	
Total accuracy	±10 W/m^2 or ± 5 %	
Resolution	1.25 W/m^2	
Drift	<±2% per year	
Air Flow sensor	**Measure range**	
Measurement range	0–5 m/s	
Operating temperature range	−20 − +60°C	
Total accuracy	± 0.2 m/s	
Start threshold	0.1 m/s	
Surface temperature sensor (for U value measure)	**Measure range**	
Total accuracy	± 0.10°C	
Resolution	0.01°C	
Measurement range	−40 − +80°C	
Heat flux sensor (for U value measure)	**Measure range**	
Measurement range	T: −40 − +80°C	HF: −1.6 − +1.6 kW/m^2
Total accuracy	T: ± 0.10°C	RH: ± 3 %
Resolution	T: 0.01°C	HF: 0.09 W/m^2

July). During daytime, as solar irradiance increases, reaching peak values between 600 and 800 W/m^2, the temperatures of the glass wool surface rise significantly. Overall, the results demonstrate that the ventilated cavity responds dynamically to solar radiation, promoting upward airflow and thermal stratification that enhance heat removal during the hottest hours of the day. The temperature differences observed along the façade height are consistent with patterns reported in similar studies on naturally ventilated or double-skin façades in temperate climates [38]. This confirms the effective operation of the buoyancy-driven ventilation mechanism and its role in improving the thermal performance of the façade system under summer conditions.

The detailed key observation are as a following:

I. The upper external cladding (T_clad$_{HF}$) reached a maximum of 61.94 °C, driven by intense solar radiation. This is the highest recorded temperature among all monitored components, highlighting the cladding's exposure and its low thermal inertia, which causes it to rapidly heat up during peak solar hours.
II. The insulation layer (fiberglass behind a black veil, T_glass$_{HF}$) reached a peak of 58.61 °C, just 3.3 °C below the outer cladding. This indicates significant heat transfer from the cladding through radiation and convection into the ventilated cavity and underlying layers.
III. The ventilated air cavity (T_vent) shows lower peak temperatures compared to the solid components. With a maximum of 48.25 °C, the air is cooler than the adjacent cladding and insulation, confirming the cooling effect of ventilation in limiting internal heat build-up.
IV. The lower cladding and glass temperatures generally register slightly lower temperature values than their upper counterparts, due to reduced solar exposure or vertical temperature gradients across the façade (T_clad$_{LF}$ = 55.52 °C, T_glass$_{LF}$ = 48.64 °C).

The results clearly show a strong correlation between solar radiation and the thermal response of the ventilated façade components.

The upper glass surface (*T_glass_HF*) reaches a maximum of approximately 58.6 °C, while the lower portions remain cooler (around 34–40 °C). This vertical temperature gradient confirms the development of buoyancy-driven airflow within the cavity, as warmer air accumulates near the upper section. The ventilated cavity air temperature (*T_vent*) follows a similar trend, peaking between 45 and 50 °C during maximum solar exposure, which is notably higher than the external air temperature (*T_amb,ext*), typically ranging between 30 and 35 °C.

During the nighttime, the façade elements cool rapidly, with temperatures across all sensors converging toward the ambient air temperature, indicating a strong diurnal thermal cycle. The observed temperature lag between the external radiation peaks and the temperature maxima of the glass surfaces suggests a moderate thermal inertia of the façade materials. This behavior highlights the façade's capacity to absorb and later release heat, which contributes to moderating indoor temperature fluctuations.

Fig. 13 illustrates the temperature distribution through the layers of the opaque ventilated façade (OVF) at 1 PM, during peak solar radiation, comparing measurements at two heights: a high-level point (dashed line) and a low-level point (dotted line).

The cladding temperature measured at the upper point (T_clad$_{HF}$) is 5.8 °C higher than that recorded at the lower point (T_clad$_{LF}$). Similarly, the outer surface temperature of the insulation layer exhibits a difference of 8.9 °C between the high-level (T_glass$_{HF}$) and low-level (T_glass$_{LF}$) measurement locations. The external cladding surface demonstrates the largest diurnal temperature variation, with fluctuations of approximately 40 °C between morning and afternoon periods. Conversely, the innermost surface of the thermal insulation exhibits the lowest thermal variability, with temperature changes limited to around 15 °C. Analysis of the temperature profiles at the cladding exterior (T_clad$_{HF}$) and the rear face of the glass wool insulation panel (T_glass$_{HB}$) reveals a thermal phase shift of approximately three hours within the ventilated façade system. Furthermore, the temperature attenuation between these two points is measured at 21.6 °C, underscoring the combined effectiveness of the ventilated air cavity and the thermal insulation layer in reducing heat transfer to the interior environment.

As soon as the solar radiation hit the surface, the temperature of all the layer increases. During hot summer days with high solar radiation, the air temperature of the inner side of the fiber glass remains lower than the ambient air temperature due a combination of shading, ventilation and the resistivity of the thermal insultation layer. Fig. 14 captures the dynamic thermal and airflow behavior within the cavity over a full 24-hour cycle, highlighting the effect of solar radiation and wind speed on the passive ventilation mechanism. As solar gains increase during the daytime, the cavity temperature rises significantly, inducing buoyancy-driven airflow that enhances air velocity. Conversely, during nighttime hours, reduced thermal gradients lead to lower temperatures and a noticeable drop in air movement. The differences in cavity air speed are due to this effect only, since the prevailing wind is not directed towards the analysed façade (Fig. 14b). This comparison demonstrates the strong coupling between thermal and fluid dynamic responses within the ventilated façade system under summer conditions.

The temperature and velocity of the air within the ventilated cavity exhibit a strong diurnal coupling, driven primarily by variations in solar radiation intensity. During daylight hours, the cavity air temperature increases significantly in response to solar gains, rising from approximately 22–24 °C in the early morning to peak values of 48–50 °C in the afternoon. This temperature rise enhances buoyancy forces within the cavity, generating upward airflow with velocities that increase from less than 0.6 m/s in the morning to peak values of 1.0–1.2 m/s during the hours of maximum solar irradiance. The positive correlation between cavity air temperature and airflow velocity (R2 ≈ 0.76) confirms the dominant influence of solar radiation on the cavity's thermal and

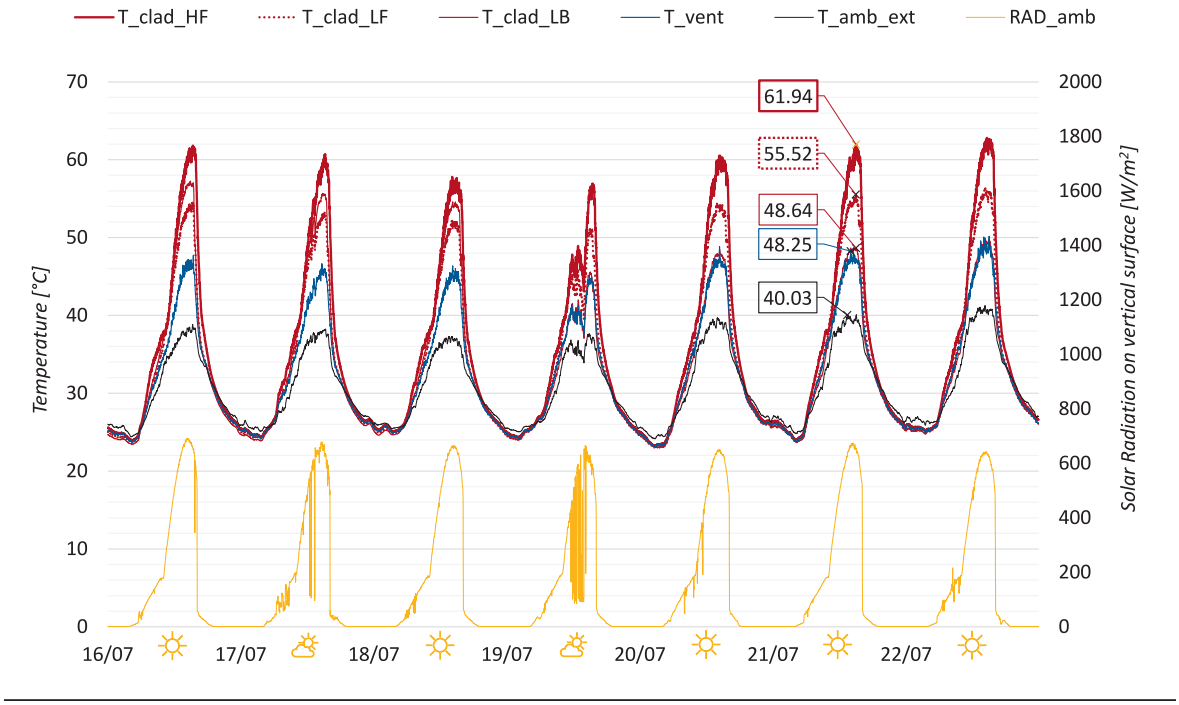

a)

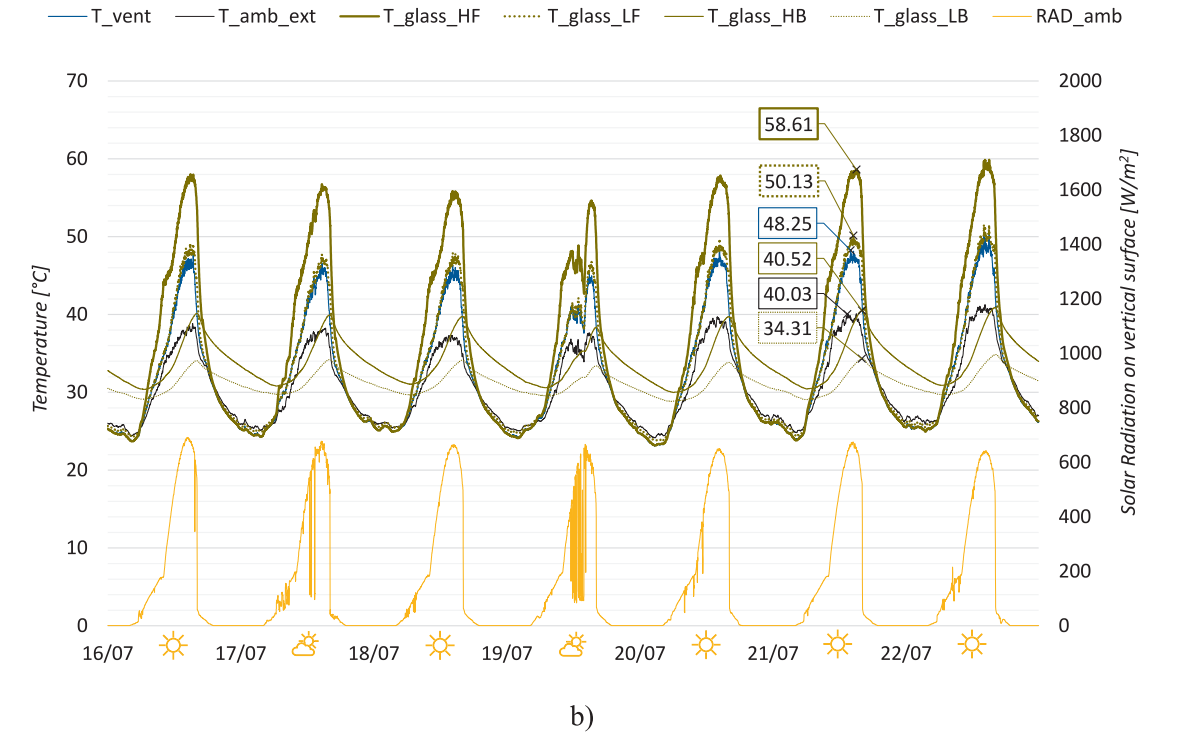

b)

Fig. 12. Temperature levels monitored through the different wall layers of the OVF between 16th – 22nd July 2023: a) external cladding; b) glass wool.

aerodynamic behavior. During peak daytime conditions, the air velocity reaches up to 1.1 m/s, corresponding to an estimated airflow rate of 481 m^3/h. In contrast, during nighttime, the absence of solar input significantly reduces the thermal gradient, leading to a marked drop in airflow. Under these conditions, the air velocity falls below 0.6 m/s, with a corresponding airflow rate of approximately 240 m^3/h.

The scatter plot of Fig. 15a) shows the correlation between cavity air speed (m/s) and cavity air temperature (°C) within the ventilated façade system during summer condition (16th–22nd of July 2023). The data points indicate a positive correlation between cavity air speed and cavity air temperature. As cavity air speed increases from approximately 0.55–1.1 m/s, the cavity air temperature tends to rise from about 25 °C to 50 °C. The air speed increases linearly in accordance with the air cavity temperature (R^2 of 0.76).

Fig. 15b) depict the correlation between the temperature level of the façade layers versus ambient air temperature. The polynomial interpolation well represents the temperature distribution with R^2 above 0.96 for the cladding, the insulation layer supporting the fact that a change in

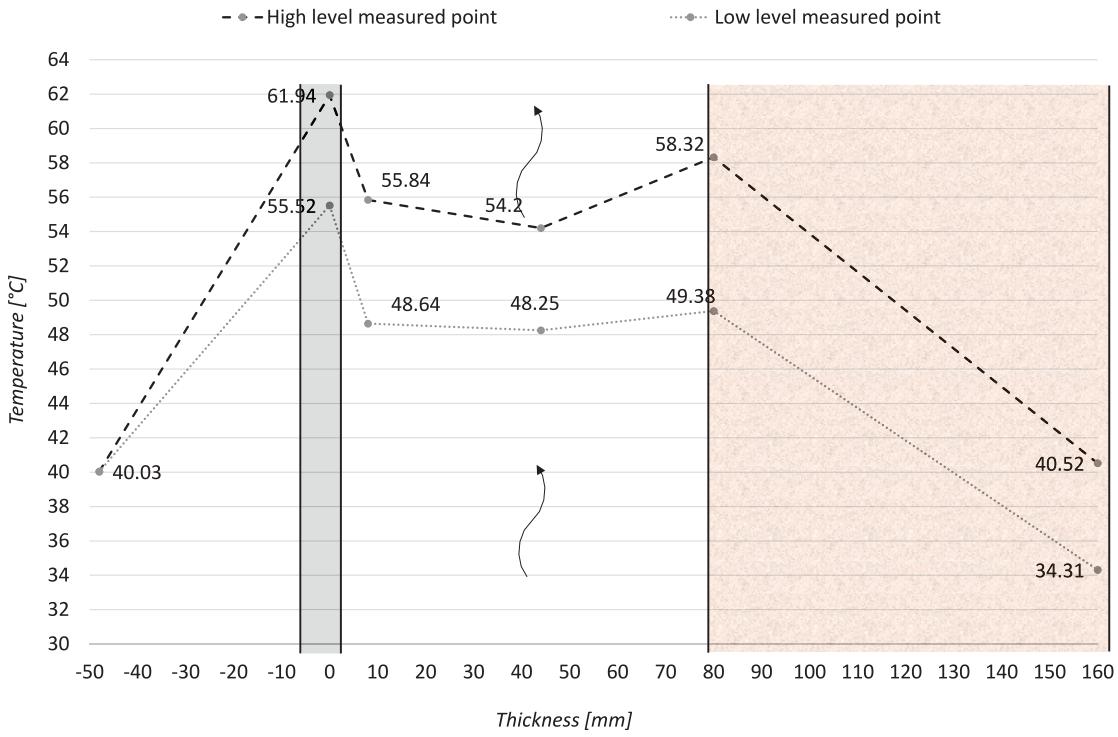

Fig. 13. Temperature profile of the bottom and top measured points of the OVF collected at 2:00 pm of July 21st.

surface temperature is not directly proportional to the change in ambient air temperature. The air cavity instead show a linear correlation with the ambient air temperature with R^2 equal to 0.969. The following consideration can be derives:

I. All surface temperatures increase as the ambient air temperature increases, showing a positive correlation.
II. The T_clad_HF (red) and T_glass_HF (yellow) lines rise steeply and have the highest surface temperatures at the upper range of ambient temperatures, reaching around 60 °C at an ambient temperature of 40 °C.
III. These two surfaces also have very high R^2 values of 0.9682 and 0.9603, respectively, indicating an excellent linear fit and strong correlation with ambient temperature.
IV. The T_vent (blue) line shows a moderate increase, with surface temperatures reaching just under 50 °C at the highest ambient temperatures. Its R^2 value of 0.9692 also indicates a strong correlation.
V. The T_glass_HB (green) line increases more slowly compared to the other surfaces and has the lowest R^2 value among the surfaces, 0.4671, indicating a weaker correlation with ambient temperature.

Fig. 16 depict the trend of the air velocity inside the OVF cavity (right) and its probability density function (left). The pattern of cavity air speed you shared aligns well with typical daily temperature variations. During the daytime, as the temperature rises (due to solar heating), the air inside the cavity heats up, causing it to expand and move faster, this leads to the peaks in air speed evident on the graph.

The probability distribution graph shows that for the most of the time the air velocity inside the cavity is in between 0.5 and 0.6 m/s, and the most frequent air velocity value, with a probability of up to 20 %, is of 0.58 m/s. The air velocity of 1 m/s has been recorded for 3 % of the time, during the hottest hours of the day. Fig. 17 compares the surface heat flux of the ventilated façade (OVF) and an unventilated façade with the same wooden structure and external insulation under the same indoor and outdoor conditions over a representative summer period (15–24 July). The internal temperature of the rooms were set to 24 °C by an automatic air-conditioning control system. The negative values of the heat fluxes indicate that the thermal energy is entering from the outside to the inside of the wall sample. The results show that the ventilated façade consistently exhibits lower heat flux values compared to the unventilated wall, indicating reduced heat transfer through the envelope. The mean heat flux of the ventilated façade is − 0.89 W/m2, while the unventilated façade records −1.83 W/m2, demonstrating an average reduction of about 51 %. Peak differences are particularly noticeable during the hottest days (e.g., 19–20 July), when the ventilated façade limits inward heat flow more effectively, with maximum reductions reaching up to approximately 5 W/m2. These results confirm the positive thermal performance of the ventilated façade system in summer conditions, improving the wall's thermal resistance and reducing cooling loads by promoting convective heat removal and reducing solar heat transfer through the building envelope.

3.2. Winter performance analysis

This section presents and discusses the experimental results of the OVF system collected during the winter season. Specifically, the data refer to a monitoring period between January 12th and January 18th, 2023, which is representative of typical local winter conditions. Fig. 18, illustrates the overall temperature trends and solar radiation levels across the different OVF wall layers during this week. In general, during overcast (cloudy) days, the temperature of the external layers of the OVF closely follows the ambient air temperature. The external cladding surface reaches peak temperatures of approximately 15–20 °C around midday (12:00–13:00), while minimum values between –0.5 °C and 1 °C are typically recorded in the early morning (around 6:00–7:00). In contrast, the inner surface of the thermal insulation layer maintains a significantly more stable and elevated temperature profile, with values consistently 8–12 °C higher than the ambient air temperature. This thermal buffer highlights the insulating performance of the wall assembly under winter conditions, minimizing heat loss toward the

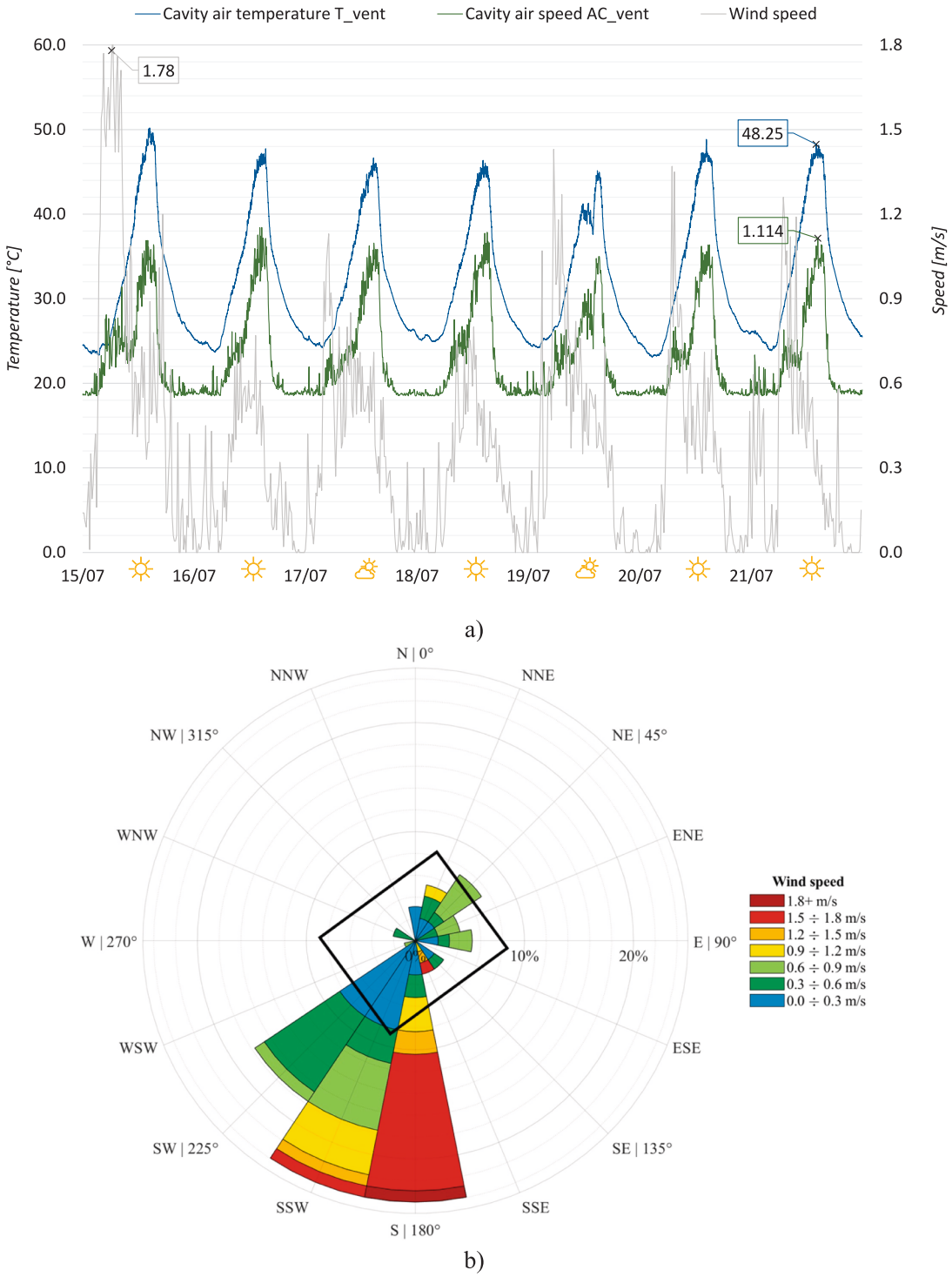

Fig. 14. Wind speed, temperatures and air velocities monitored inside the OVF cavity between 15th and 21st of July 2023: a) weekly trend; b) wind rose of the 15th of July 2023 highlighting in black the orientation of BEE Lab.

exterior.

Fig. 18 includes for a more clear data interpretation, the surface temperature of the different OVF layers recorded during January 18th 2023, under typical winter weather conditions. During sunny winter days, the external surface temperature of the cladding panels exhibits a diurnal variation of approximately 16 °C, with peak values ranging between 17 °C and 20 °C. A vertical temperature gradient is observed across the façade, consistent with the behavior noted during the summer monitoring phase. Specifically, the upper part of the façade (T_clad_HF) recorded a maximum surface temperature of 17.7 °C, while the lower section (T_clad_LF) reached only 13.9 °C, indicating a difference of 3.8 °C. A similar pattern was observed in the thermal insulation layer: the outer surface at the upper measurement point (T_glass_HF) reached 17.6 °C, compared to 11.27 °C at the lower point (T_glass_LF), resulting in a temperature difference of 6.33 °C. In contrast, the inner surface temperatures of the insulation layer (T_glass_HB and T_glass_LB), positioned closer to the interior, showed minimal variation throughout the day. These temperatures remained relatively stable, with values ranging

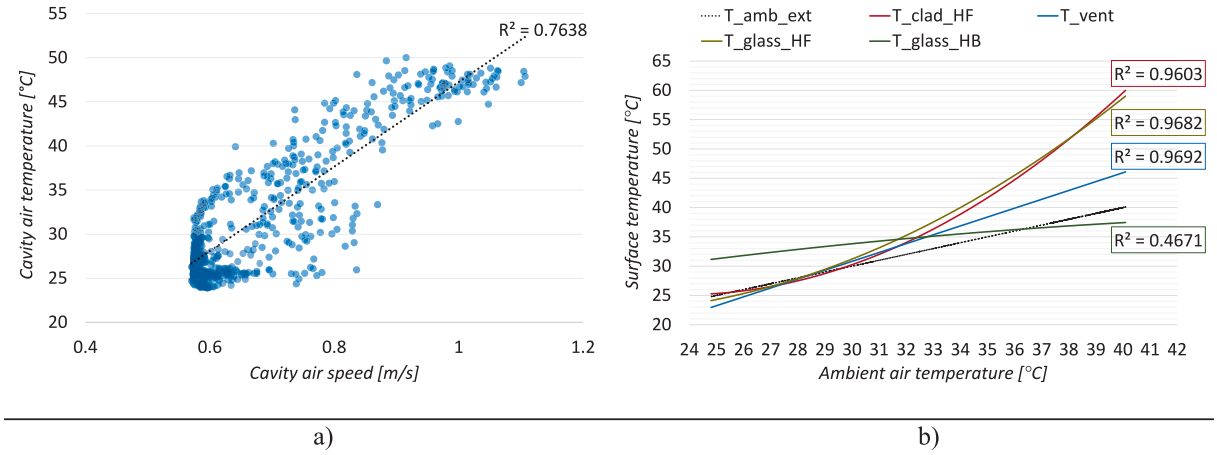

Fig. 15. OVF temperature correlation data analysis – July 22nd 2023: a) correlation between the cavity air temperature and the cavity air speed; b) correlation between the surface temperature of the OFV layers and the ambient air temperature.

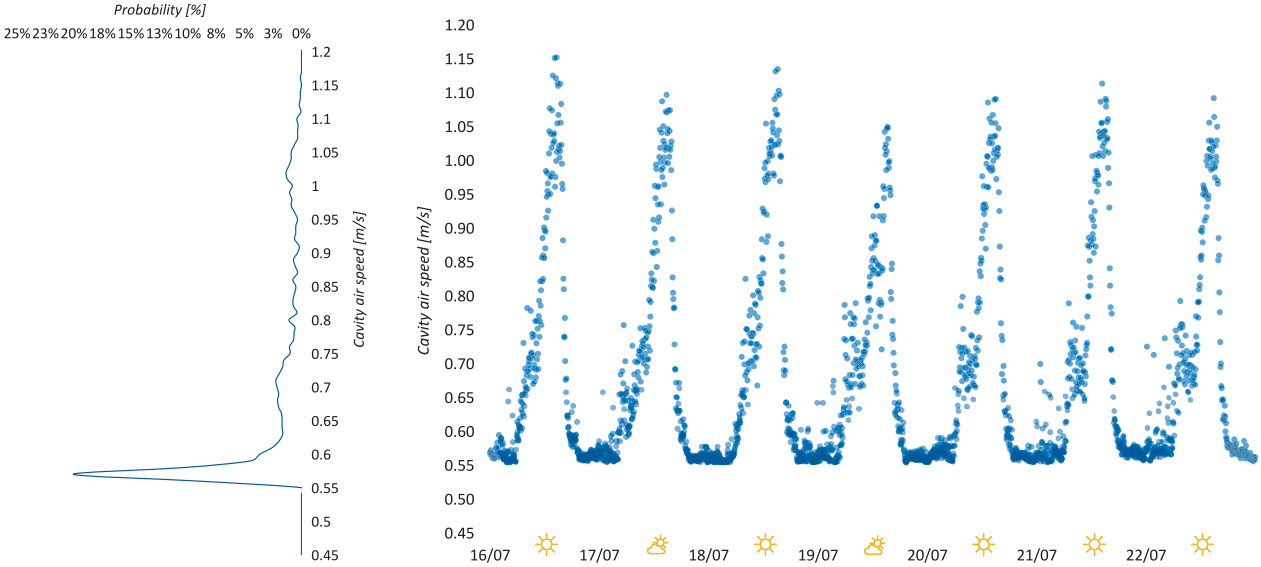

Fig. 16. Air flow inside the OVF cavity (right) and probability distribution (left) of the week 16th to 22nd of July 2023.

between 9 °C and 12 °C, demonstrating the thermal buffering capacity of the multi-layered façade system. Fig. 19 shows the temperature distribution across the façade thickness measured at 1 pm, comparing two points at different heights: a high-level point (dashed line) and a low-level point (dotted line). As observed in the summer dataset, at peak solar exposure, the façade's upper section shows significantly higher temperatures at the outer surfaces compared to the lower section, reflecting greater solar radiation exposure. However, this difference diminishes within the insulation layer, where temperatures become more uniform, indicating effective thermal insulation and heat transfer reduction toward the interior.

Fig. 20 presents the relationship over time between cavity air temperature and the cavity air speed between the 12th and the18th of January 2023, comparing cavity air speed to wind speed. The graph displays a week linear dependence between the two variables indicating that the temperature of the air cavity still below the minimum threshold for activating the buoyancy effect. The cavity air speed during the recording time shows values in the range 1.0–0.49 m/s. The higher values are due to the wind pressure distribution on the façade and are not due to the airflow buoyancy effect.

Fig. 21 analyses the correlation between the air temperature of the OVF cavity and: a) the cavity air speed and, b) the external ambient air temperature during the cold season. The recorded air speed shows a weak correlation with the air cavity temperature (R^2 of 0.27). The air speed values, instead, depends more by the local weather condition like the wind direction, intensity and pressure created on the façade. As shown for the summer season, a polynomial correlation between air and the cladding surface temperature suggests a non-linear relationship, the change in surface temperature is not directly proportional to the change in air temperature, but rather follows a polynomial of 2° order curve. The air cavity instead show a linear correlation with the ambient air temperature with R^2 equal to 0.958.

Fig. 22 gives an accurate picture of the trend of the air velocity in the OVF cavity (right) and its probability density function (left), to highlight the air velocity probability during the experimental measures. The figure, in particular, demonstrates that the most prevalent air velocity in the cavity is approximately 0.55 m/s, with a probability of 5.85 %. This value is predominantly observed during the nighttime hours.

The Fig. 23 presents the comparison of surface heat flux between the ventilated façade (OVF) and an unventilated façade with the same wooden structure and external insulation under the same indoor and outdoor conditions during a representative winter period (12–17

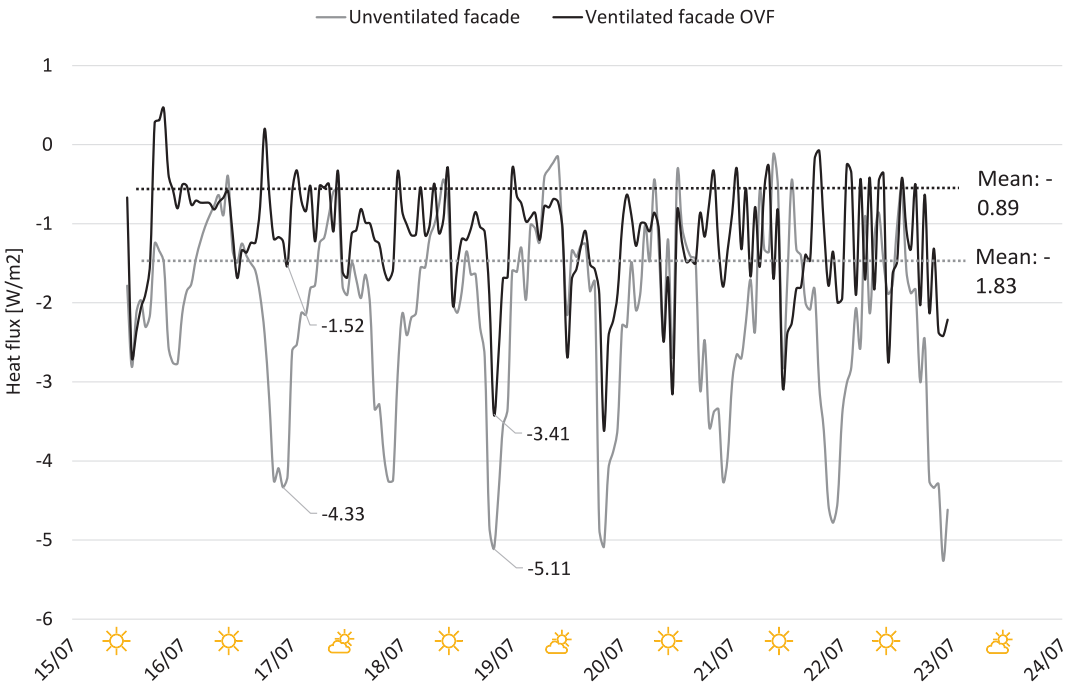

Fig. 17. Heat fluxes (W/m2) measured for both the OVF and the unventilated façade during four summer days (16th and the 19th of July 2023). The mean heat flux of the ventilated façade is − 0.89 W/m2, while the unventilated façade records −1.83 W/m2.

January).. The internal temperature of the test rooms were set to 22 °C by through automatic air temperature control system.

The positive values of the heat fluxes indicate that the thermal energy is moving from inside to the outside of the building envelope. Throughout the monitoring period, the unventilated façade shows higher heat flux values, indicating greater heat losses through the wall. The mean heat flux of the unventilated façade is 3.32 W/m2, whereas the ventilated façade records a lower mean value of 2.52 W/m2, corresponding to a reduction of approximately 24 %. Peak differences are observed during the coldest days (e.g., 13–14 January), when the ventilated façade limits outward heat transfer, with minimum values as low as 1.15 W/m2 compared to 4.27 W/m2 for the unventilated façade. These results confirm that the ventilated façade effectively enhances the wall's thermal performance in winter, reducing heat losses and contributing to improved energy efficiency under heating-dominated conditions.

3.3. *Design implications and guidelines*

The selection of an optimal opaque ventilated façade (OVF) configuration necessitates a comprehensive evaluation of multiple factors, including local climatic conditions, façade construction technology, building orientation, functional use, maintenance strategies, and targeted occupant comfort levels. Other than analysing the climate and indoor conditions under which the OVF operates, it is therefore necessary to carefully design the façade itself. In particular, the OVF outermost layers should be able to reach temperature differentials sufficient to induce buoyancy effects without significant thermal cycling to avoid high thermal stress which could potentially compromise façade durability and lead to aesthetic degradation. It is also critical to select finishing materials characterized by high reflectivity (e.g., high albedo and *retro*-reflective properties) to optimize thermal performance and avoid excessive heat absorption. The thickness and thermal inertia of the cladding should be selected based on the required cooling effectiveness of this layer, since this cladding panels with low thermal inertia limit this effect. Air cavity thickness, instead, should balance local meteorological conditions and materials surface radiative properties to induce an effective stack effect within the air cavity.

The ventilated façade technology is expected to contribute to a NZE building by reducing overall heat losses through the building envelope, thereby lowering heating demand during cold periods and the cooling demand during summer time. Specifically, the investigated ventilated façade achieves a U-value of 0.13 W/m^{2}K (compared to 0.19 W/m^{2}K for the unventilated façade) that is in the range values required for Zero Energy Building in typical Cfb climate.

4. Conclusions

The study presents and discusses the results of a long-term experimental monitoring campaign conducted to characterize the OVF. The experimental tests were performed in the BEE Lab (Building façadE performancE Lab) outdoor test cell facility at Politecnico di Milano, Lecco campus, Italy. The laboratory has been developed within the context of the EU funded H2020 project MEZroE which aims to create an Open Innovation Digital Platform for Zero Energy Building Ecosystem to accelerate the energy transition in the building sector by driving the advancement of low- impact, energy-efficient solutions from open innovation collaboration to the market. The results contribute to the available scientific literature reporting evidence regarding the real performance analysis of a specific façade technology representing, from the geometrical point of view, one of the main common OVF on the market. Although this study focuses on a specific opaque ventilated façade (OVF) configuration, the façade assessment yields several broadly relevant insights. Specifically, the research enabled: i) the experimental characterization of temperature distribution across the distinct OVF layers under both high summer and low winter ambient conditions; ii) the analysis of the relationship between façade temperature profiles and air velocity within the OVF cavity during varying seasonal periods; and iii) the validation of the stack effect phenomenon in typical low-ventilation OVF systems across diverse meteorological conditions. The experimental findings highlight the intrinsic complexity of OVF thermal behavior, which poses challenges for comprehensive performance evaluation due to the multitude of interacting variables influencing overall system dynamics. Furthermore, the results

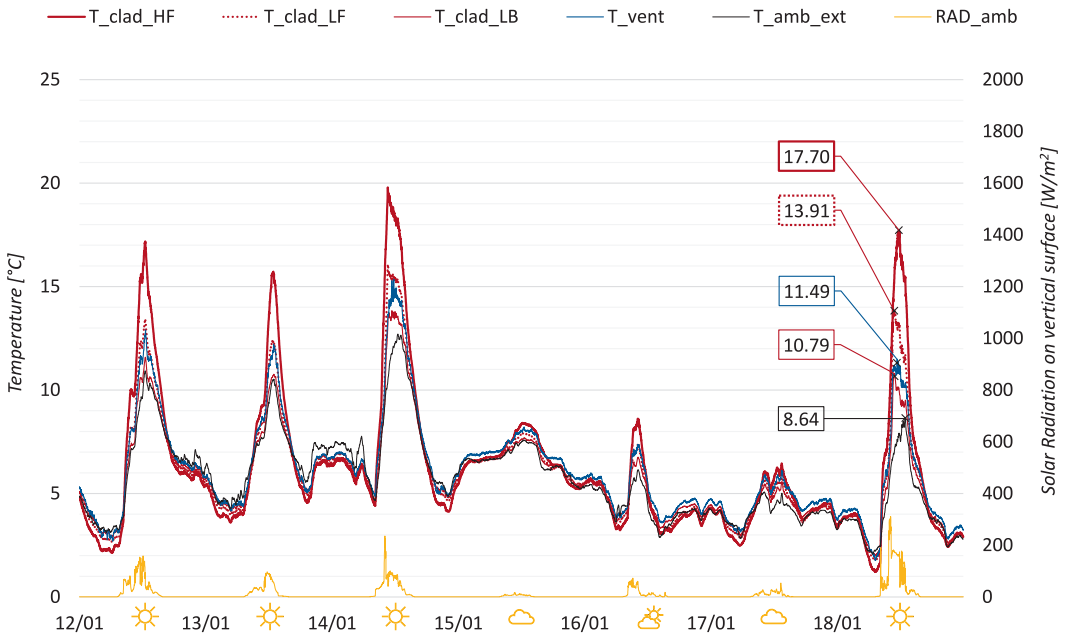

a)

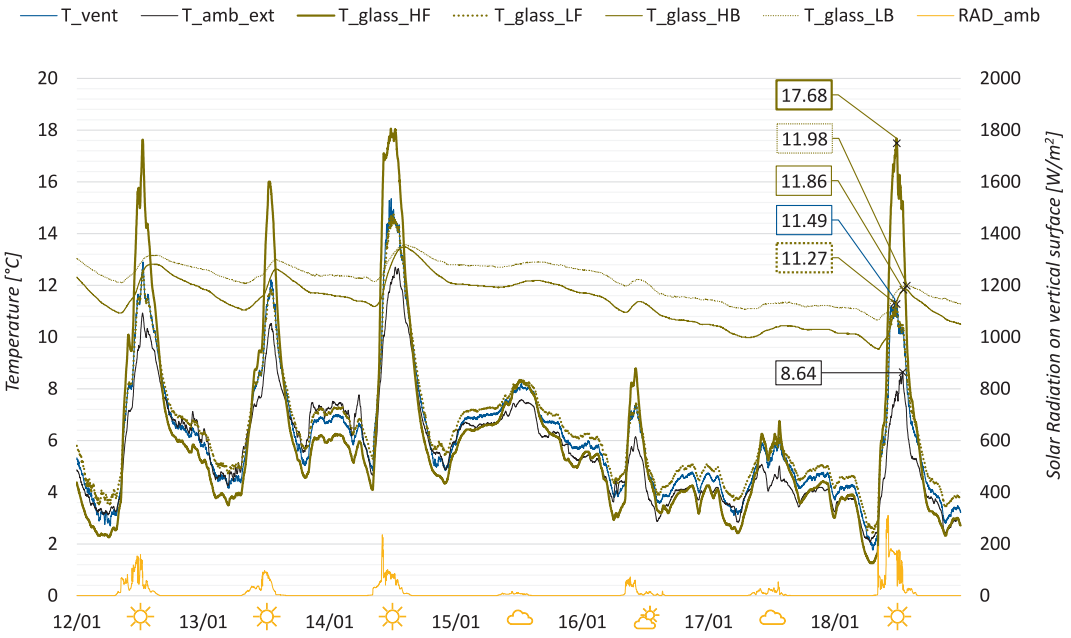

b)

Fig. 18. Temperature values monitored through the different layers of the OVF during the week from 12th to 18th of January 2023. The solar radiation intensity is represented by the orange line on the right axis: a) external cladding; b) glass wool. (For interpretation of the references to colour in this figure legend, the reader is referred to the web version of this article.)

substantiate the significant influence of local microclimatic factors on OVF performance. Based on the specific monitoring campaign of the investigated façade, the main outcomes can be summarized as follows:

- During summer the differential between peak and minimum surface temperatures of the outermost layers is approximately 38 °C, while the shading effect provided by the cladding reduces the temperature of the cavity thermal insulation of about 3.5–5 °C. Moreover, a strong linear correlation ($R^2 = 0.76$) is observed between air velocity and temperature inside the ventilated cavity. The average heat flux of the OVF shows a reduction of approximately 51 % compared to the one

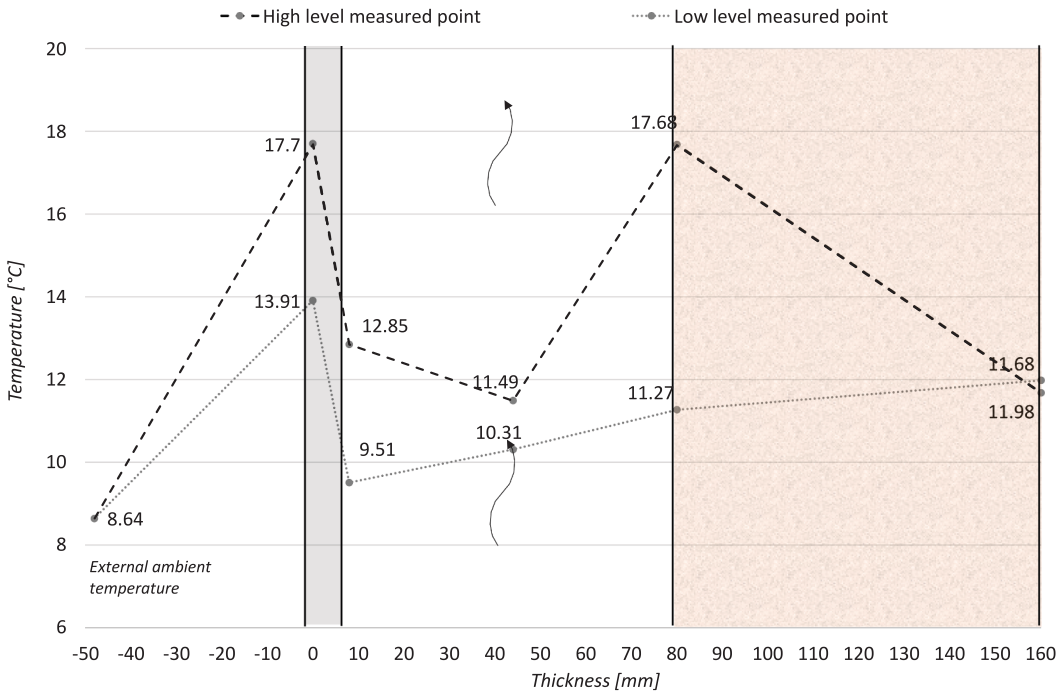

Fig. 19. Temperature profile of the bottom and top measured points of the OVF recorded at 1:00 pm on January 18th.

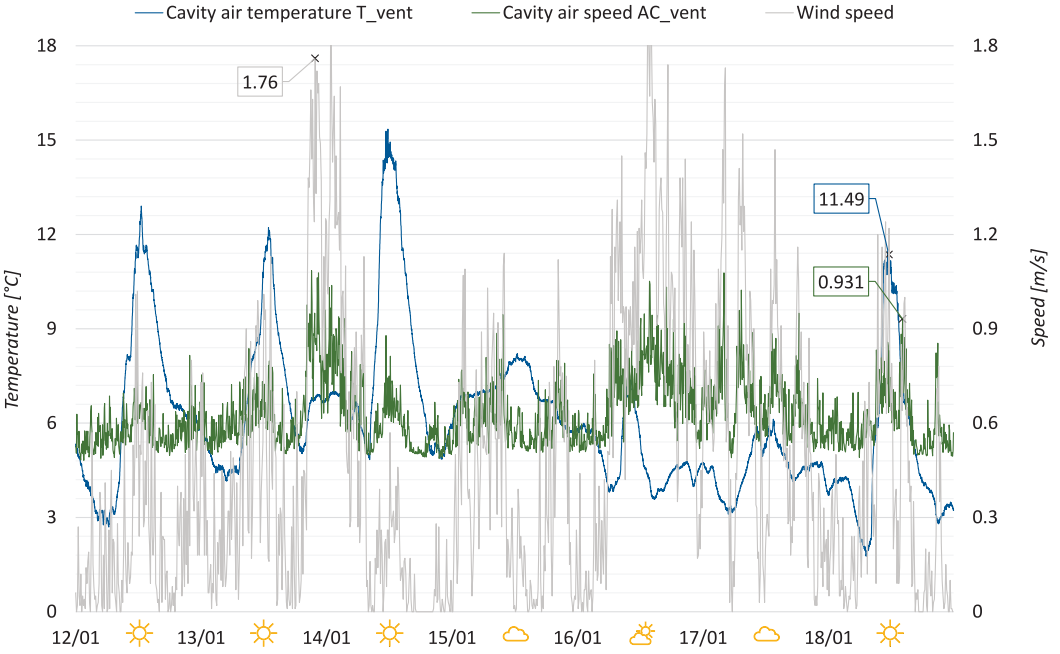

Fig. 20. Wind speed, temperatures and air velocities monitored inside the OVF cavity between January 12th −18th 2023.

of an unventilated façade with the same wooden structure and external insulation.

- During winter sunny days cavity air velocity ranges from 0.48 m/s to 1.0 m/s and cavity air temperature is higher than the ambient one of about 3–4 °C, while with limited solar radiation cavity air velocity is stable under 0.4 m/s and cavity air temperature closely follows ambient air temperature. Moreover, the average heat flux of the OVF shows a reduction of approximately 24 % compared to the one of an unventilated façade with the same wooden structure and external insulation.
- In both summer and winter seasons moderate vertical temperature stratification is observed within the OVF from the bottom to the top of the wall, with a negligible stack effect within the air cavity likely due to the limited air cavity thickness (70 mm). The correlation between ambient air temperature and cavity air temperature follows a second-order polynomial trend with coefficients of determination $R^2 = 0.96$ in summer and $R^2 = 0.94$ in winter.
- The performance of the monitored OVF aligns well with values reported in previous experimental and simulation studies carried out on common façade systems in similar temperate climates. Double-skin façades and ventilated rainscreen systems typically achieve

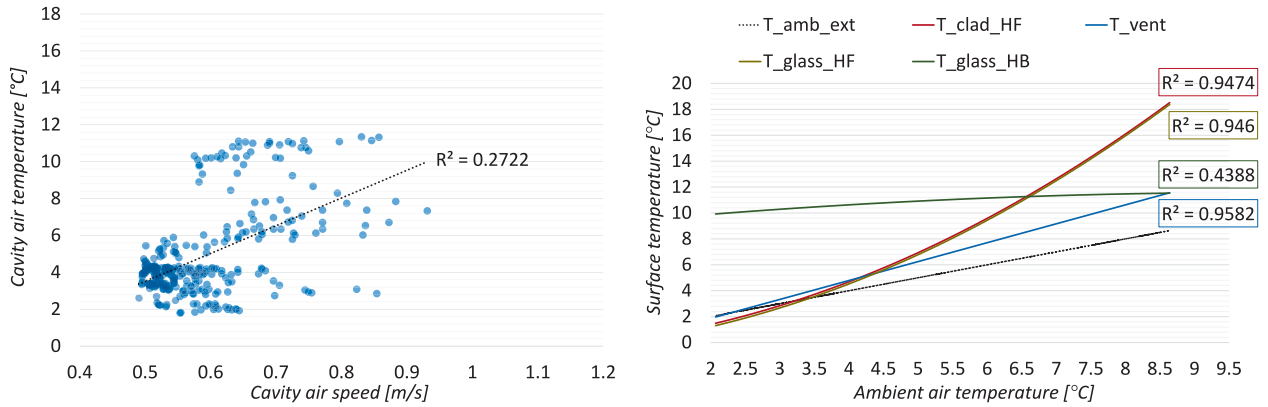

Fig. 21. OVF temperature correlation data analysis – January 18th 2023: a) correlation between the cavity air temperature and the cavity air speed; b) correlation between the surface temperature of the OFV layers and the ambient air temperature.

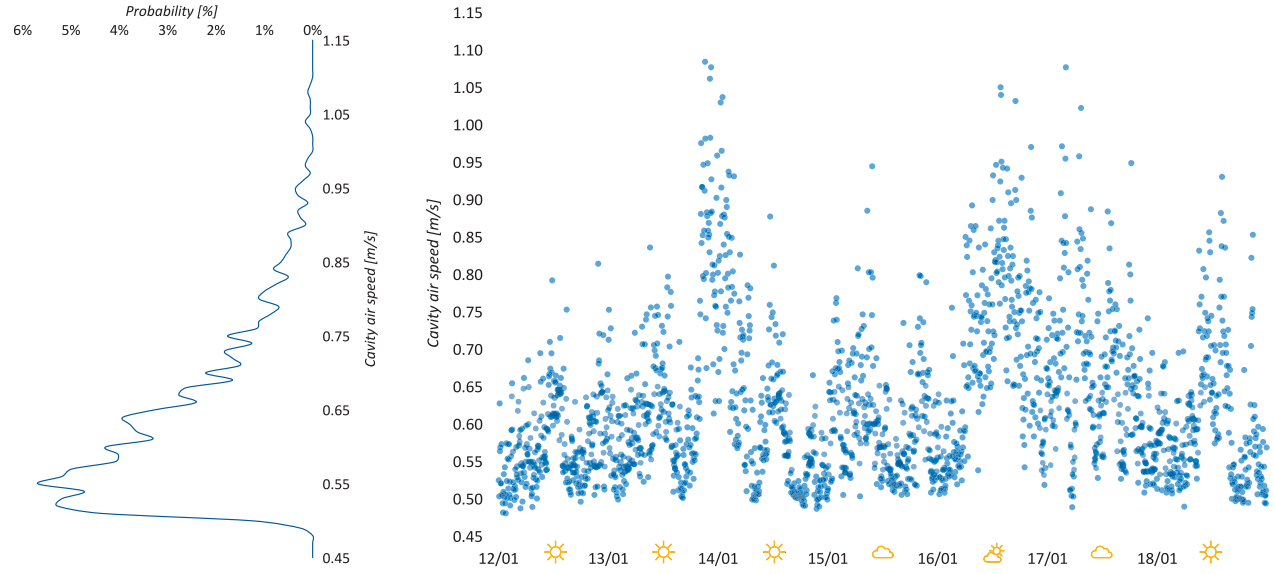

Fig. 22. Cavity air speed analysis of the OVF cavity (right) and the related probability density function (left) The data refers to the time between the 12th and 18th of January 2023.

summer heat flux reductions of 40–60 % and winter heat loss reductions of 20–30 % with respect to conventional solid walls [39,40,51]. The observed performance of the OVF thus falls within the upper range of these benchmarks, confirming its effectiveness as a passive strategy for improving thermal regulation. Moreover, the dynamic behavior of the OVF—characterized by strong responsiveness to solar radiation and outdoor air temperature—suggests that the system could provide additional benefits in mixed climates by reducing both cooling and heating demands throughout the year. Overall, the monitored results indicate that the OVF performs comparably or slightly better than other ventilated façade configurations reported in the literature for similar climatic conditions [30,41,42,52], demonstrating its potential for energy-efficient building envelope design and retrofitting applications.

Since the performance of OVF systems exhibits significant variability across different climatic zones, urban contexts, and microclimatic environments due to the pronounced influence of localized weather patterns on thermal and airflow dynamics, the experimental data presented herein provide valuable empirical benchmarks for architects and engineers, enabling the prediction of thermal and aerodynamic behavior of OVFs with analogous geometric configurations and material finishes. These findings can serve as an essential reference during the preliminary design phases to optimize façade performance and ensure contextual suitability, but at the same time similar future research and studies on different OVF configurations using other cladding systems are required to provide complete guidelines to designers. Future work will need to evaluate more testing scenarios to analyse the performance of OVFs under different indoor/outdoor conditions and at different orientations.

CRediT authorship contribution statement

Graziano Salvalai: Writing – review & editing, Writing – original draft, Visualization, Validation, Methodology, Investigation, Funding acquisition, Formal analysis, Data curation, Conceptualization.

Funding

The present research has been carried in the contest of MEZeroE project (Measuring Envelope products and systems contributing to next generation of healthy nearly Zero Energy Buildings) funded by the European Union's Horizon 2020 research and innovation programme under grant agreement N° 953157.

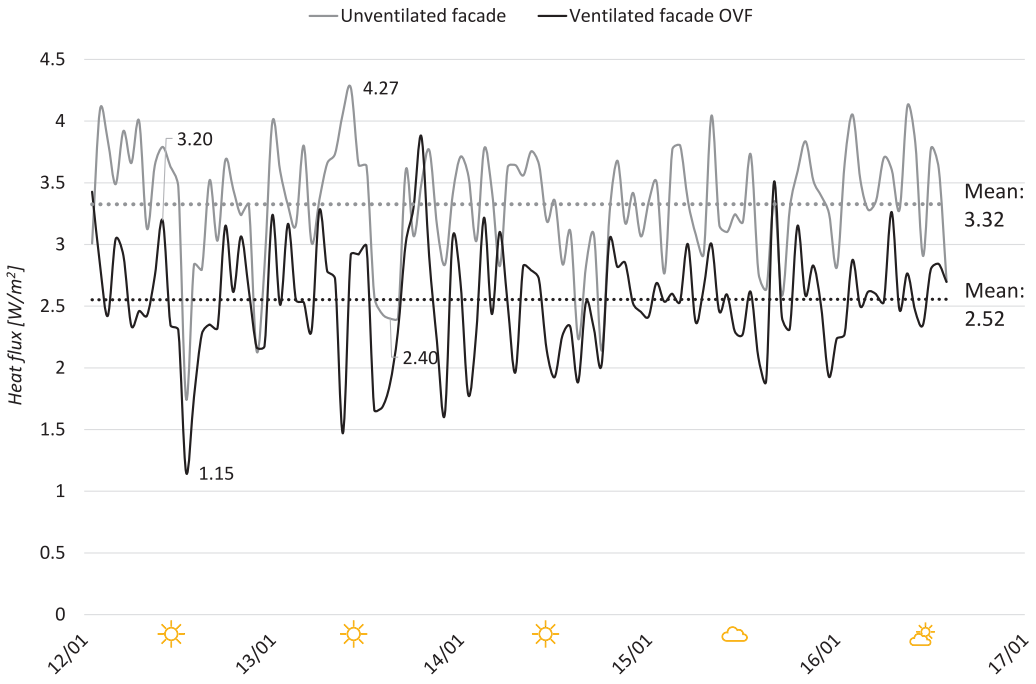

Fig. 23. Heat fluxes intensity (W/m2) passing through the wall for both the OVF (and the unventilated façade during the winter experimental campaign, between January 12th and January16th, 2023.

Declaration of Competing Interest

The author declare that he have no known competing financial interests or personal relationships that could have appeared to influence the work reported in this paper.

Data availability

No - I have not included a data availability in my manuscript

References

[1] European Commission, D.-G. for E. COMMUNICATION FROM THE COMMISSION TO THE EUROPEAN PARLIAMENT, THE COUNCIL, THE EUROPEAN ECONOMIC AND SOCIAL COMMITTEE AND THE COMMITTEE OF THE REGIONS A Renovation Wave for Europe - Greening Our Buildings, Creating Jobs, Improving Lives; Brussels, 2019.

[2] Energy EU Policies Aim to Deliver Secure, Sustainable and Affordable Energy for Citizens and Businesses.

[3] European Commission, D.-G. for E. COMMUNICATION FROM THE COMMISSION TO THE EUROPEAN PARLIAMENT, THE COUNCIL, THE EUROPEAN ECONOMIC AND SOCIAL COMMITTEE AND THE COMMITTEE OF THE REGIONS A Renovation Wave for Europe - Greening Our Buildings, Creating Jobs, Improving Lives 2020.

[4] European Commission Directive (EU) 2024/1275 of the European Parliament and of the Council of 24 April 2024 on the Energy Performance of Buildings (Recast); Official Journal of the European Union: European Union, 2024.

[5] IEA Building Envelopes. *IEA* 2023.

[6] M. Ibañez-Puy, M. Vidaurre-Arbizu, J.A. Sacristán-Fernández, C. Martín-Gómez, Opaque Ventilated Façades: thermal and Energy Performance Review, Renew. Sustain. Energy Rev. 79 (2017) 180–191, https://doi.org/10.1016/J.RSER.2017.05.059.

[7] S. Xu, C. Li, W. He, W. Chu, Z. Hu, B. Lu, Experimental Study of Bifacial Photovoltaic Wall System Incorporating Thermochromic Material, Sustain. Cities Soc. 106 (2024) 105372, https://doi.org/10.1016/j.scs.2024.105372.

[8] O. Zhao, W. Zhang, M. Chen, L. Xie, J. Li, Z. Li, J. Zhong, X. Wu, Experimental and Numerical Study on the Performance of innovative Bifacial Photovoltaic Wall System, Sustain. Cities Soc. 85 (2022) 104085, https://doi.org/10.1016/j.scs.2022.104085.

[9] D. Garraín, I. Herrera, I. Rodríguez-Serrano, Y. Lechón, A. Hepbasli, M. Araz, E. Biyik, R. Yao, M. Shahrestani, E. Essah, et al., Sustainability Indicators of a naturally Ventilated Photovoltaic Façade System, J. Clean. Prod. 266 (2020) 121946, https://doi.org/10.1016/j.jclepro.2020.121946.

[10] A.C.F. Maciel, M.T. Carvalho, Operational Energy of Opaque Ventilated Façades in Brazil, J. Build. Eng. 25 (2019) 100775, https://doi.org/10.1016/j.jobe.2019.100775.

[11] Karanafti, A.; Theodosiou, T.; Tsikaloudaki, K. Improving the Cooling Performance of an Opaque Ventilated Facade Using an Airflow Network Model for the Mediterranean Climate. In Proceedings of the 2023 8th International Conference on Smart and Sustainable Technologies (SpliTech); IEEE, June 20 2023; pp. 1–6.

[12] S. Sarihi, F. Mehdizadeh Saradj, M. Faizi, A critical Review of Façade Retrofit measures for Minimizing heating and Cooling demand in existing buildings, Sustain. Cities Soc. 64 (2021) 102525, https://doi.org/10.1016/j.scs.2020.102525.

[13] O. Roig, C. Pardal, A. Isalgue, I. Paricio, Energy Performance of Ventilated Façades; the Influence of the Colour and the Air Channel Dimension, J. Phys. Conf. Ser. 2600 (2023) 092021, https://doi.org/10.1088/1742-6596/2600/9/092021.

[14] C. Arkar, S. Domjan, S. Medved, Lightweight Composite Timber Façade Wall with improved thermal Response, Sustain. Cities Soc. 38 (2018) 325–332, https://doi.org/10.1016/j.scs.2018.01.011.

[15] C. Marinosci, G. Semprini, G.L. Morini, Experimental Analysis of the Summer thermal Performances of a naturally Ventilated Rainscreen Façade Building, Energy Build. 72 (2014) 280–287, https://doi.org/10.1016/j.enbuild.2013.12.044.

[16] R.F. De Masi, V. Festa, A. Gigante, S. Ruggiero, G.P. Vanoli, Experimental Analysis of Grills Configuration for an Open Joint Ventilated Facade in Summertime, J. Build. Eng. 54 (2022) doi:10.1016/j.jobe.2022.104608.

[17] R.F. De Masi, S. Ruggiero, G.P. Vanoli, Hygro-thermal Performance of an Opaque Ventilated Façade with Recycled Materials during Wintertime, Energy Build. 245 (2021) 110994, https://doi.org/10.1016/j.enbuild.2021.110994.

[18] F. Stazi, G. Ulpiani, M. Pergolini, C. Di Perna, M. D'Orazio, The Role of Wall Layers Properties on the thermal Performance of Ventilated Facades: Experimental Investigation on Narrow-Cavity Design, Energy Build. 209 (2020) 109622, https://doi.org/10.1016/j.enbuild.2019.109622.

[19] O. Roig, S. Summa, C. Pardal, A. Isalgue, C. Di Perna, F. Stazi, Opaque Ventilated Façades: Energy Performance for Different Main Walls and Claddings, Energy Build. 314 (2024) 114280, https://doi.org/10.1016/j.enbuild.2024.114280.

[20] F. Petresevics, B. Nagy, FEM-Based Evaluation of the Point thermal Transmittance of Various Types of Ventilated Façade Cladding Fastening Systems, Buildings 12 (2022) 1153, https://doi.org/10.3390/buildings12081153.

[21] R. Ingeli, J. Gašparík, L. Paulovičová, Impact of an innovative solution for the Interruption of 3-D Point thermal Bridges in buildings on Sustainability, Sustainability 13 (2021) 11561, https://doi.org/10.3390/su132111561.

[22] H. El-Sadi, F. Haghighat, A. Fallahi, CFD Analysis of Turbulent Natural Ventilation in Double-Skin Façade: thermal Mass and Energy Efficiency, J. Energy Eng. 136 (2010) 68–75, https://doi.org/10.1061/(ASCE)EY.1943-7897.0000026.

[23] C. Ding, T. Ngo, R. Lumantarna, P. Mendis, M. Zobec, Investigations of Cavity pressure Behaviors of Double-Skin Façade Systems Subjected to Blast Loads, J. Perform. Constr. Fac. 29 (2015), https://doi.org/10.1061/(ASCE)CF.1943-5509.0000674.

[24] A. Gagliano, F. Nocera, S. Aneli, Thermodynamic Analysis of Ventilated Façades under Different Wind Conditions in Summer period, Energy Build. 122 (2016) 131–139, https://doi.org/10.1016/J.ENBUILD.2016.04.035.
[25] A. Gagliano, S. Aneli, Analysis of the Energy Performance of an Opaque Ventilated Façade under Winter and Summer Weather Conditions, Sol. Energy 205 (2020) 531–544, https://doi.org/10.1016/J.SOLENER.2020.05.078.
[26] J. Santa Cruz Astorqui, C. Porras-Amores, Ventilated Façade with double Chamber and Flow Control Device, Energy Build. 149 (2017) 471–482, https://doi.org/10.1016/j.enbuild.2017.04.063.
[27] M. Ciampi, F. Leccese, G. Tuoni, Ventilated Facades Energy Performance in Summer Cooling of buildings, Sol. Energy 75 (2003) 491–502, https://doi.org/10.1016/J.SOLENER.2003.09.010.
[28] E. Iribar-Solaberrieta, C. Escudero-Revilla, M. Odriozola-Maritorena, A. Campos-Celador, C. García-Gáfaro, Energy Performance of the Opaque Ventilated Facade, Energy Procedia 78 (2015) 55–60, https://doi.org/10.1016/J.EGYPRO.2015.11.114.
[29] F. Gökşen, İ. Ayçam, Thermal Performance Assessment of Opaque Ventilated Façades for Residential buildings in Hot Humid Climates, Gradjevinar 75 (2023) 225–237, https://doi.org/10.14256/JCE.3576.2022.
[30] F. Peci López, R. de Adana, M. Santiago, Sensitivity Study of an Opaque Ventilated Façade in the Winter season in different climate zones in Spain, Renew. Energy 75 (2015) 524–533, https://doi.org/10.1016/J.RENENE.2014.10.031.
[31] S. Fantucci, V. Serra, C. Carbonaro, An Experimental Sensitivity Analysis on the Summer thermal Performance of an Opaque Ventilated Façade, Energy Build. 225 (2020) doi:10.1016/j.enbuild.2020.110354.
[32] F. Stazi, G. Ulpiani, M. Pergolini, D. Magni, C. Di Perna, Experimental Comparison between three Types of Opaque Ventilated Facades, Open Constr. Build. Technol. J. 12 (2018) 296–308, https://doi.org/10.2174/1874836801812010296.
[33] S. Soudian, U. Berardi, Experimental Performance Evaluation of a Climate-Responsive Ventilated Building Façade, J. Build. Eng. 61 (2022) 105233, https://doi.org/10.1016/j.jobe.2022.105233.
[34] Z. Lin, Y. Song, Y. Chu, An Experimental Study of the Summer and Winter thermal Performance of an Opaque Ventilated Facade in Cold Zone of China, Build. Environ. 218 (2022) 109108, https://doi.org/10.1016/J.BUILDENV.2022.109108.
[35] I. Guillén, V. Gómez-Lozano, J.M. Fran, P.A. López-Jiménez, Thermal Behavior Analysis of Different Multilayer Façade: Numerical Model versus Experimental Prototype, Energy Build. 79 (2014) 184–190, https://doi.org/10.1016/J.ENBUILD.2014.05.006.
[36] S. Yadav, C. Hachem-Vermette, Comprehensive Assessment of double Skin Façades: a Mathematical Model for evaluating Influence of KL Ratio on Electrical and thermal Performances, and Indoor Conditions, Energy Build. 303 (2024) 113762, https://doi.org/10.1016/j.enbuild.2023.113762.
[37] G. Aruta, F. Ascione, N. Bianco, T. Iovane, G.M. Mauro, A Responsive Double-Skin Façade for the Retrofit of existing buildings: Analysis on an Office Building in a Mediterranean climate, Energy Build. 284 (2023) 112850, https://doi.org/10.1016/j.enbuild.2023.112850.
[38] S.W. Lee, J.S. Park, Evaluating thermal Performance of Double-Skin Facade using Response factor, Energy Build. 209 (2020) 109657, https://doi.org/10.1016/j.enbuild.2019.109657.
[39] U.-J. Sung, S.-H. Kim, A Study on the Improvement of Double-Skin Facade operation for reducing heating load in Winter, Sustainability 11 (2019) 6238, https://doi.org/10.3390/su11226238.
[40] A. Aksamija, Thermal, Energy and Daylight Analysis of Different Types of double Skin Facades in Various Climates, J. Facade Des. Eng. 6 (2018) 1–39, https://doi.org/10.7480/jfde.2018.1.1527.
[41] A. Karanafti, T. Theodosiou, Summer thermal Performance Analysis of an Opaque Ventilated Façade Operating under the Dynamic Insulation Principle, Energy Build. 312 (2024) 114193, https://doi.org/10.1016/j.enbuild.2024.114193.
[42] E. Iavorschi, L.D. Milici, C. Ungureanu, C. Bejenar, A Comparative Evaluation of the thermal Performance of Passive Facades with Variable Cavity Widths for Near-Zero Energy buildings (NZEB): a Modeling Study, Appl. Sci. 15 (2025) 7019, https://doi.org/10.3390/app15137019.
[43] M. Rahiminejad, D. Khovalyg, Review on Ventilation rates in the Ventilated Air-Spaces behind Common Wall Assemblies with External Cladding, Build. Environ. 190 (2021) 107538, https://doi.org/10.1016/j.buildenv.2020.107538.
[44] M. Rahiminejad, A. Louis Marie Pâris, H. Ge, D. Khovalyg, Performance of Lightweight and Heavyweight Building Walls with naturally Ventilated Passive and active Facades, Energy Build. 256 (2022) 111751, https://doi.org/10.1016/j.enbuild.2021.111751.
[45] R.F. De Masi, V. Festa, S. Ruggiero, G.P. Vanoli, Environmentally Friendly Opaque Ventilated Façade for Wall Retrofit: one Year of in-Field Analysis in Mediterranean climate, Sol. Energy 228 (2021) 495–515, https://doi.org/10.1016/j.solener.2021.09.063.
[46] M. Fazzini, C. Baresi, C. Bisci, C. Bna, A. Cecili, A. Giuliacci, S. Illuminati, F. Pregliasco, E. Miccadei, Preliminary Analysis of Relationships between COVID19 and climate, Morphology, and Urbanization in the Lombardy Region (Northern Italy), Int. J. Environ. Res. Public Health 17 (2020) 6955, https://doi.org/10.3390/ijerph17196955.
[47] MEZeroE H2020 Project Measuring Envelope Systems for Zero Energy Buildings Available online: https://www.mezeroe.eu/ (accessed on 28 October 2025).
[48] G. Salvalai, M.M. Sesana, P. Dell'Oro, D. Brutti, Open Innovation for the Construction Sector: Concept Overview and Test Bed Development to boost Energy-Efficient Solutions, Energies (basel) 16 (2023) 5522, https://doi.org/10.3390/en16145522.
[49] M. Colombo, G. Salvalai, D. Brutti, C.R. Depaolini, Mechanical, thermal and Durability Performance Characterization of Novel Acrylic Solid Surface Cladding Panels in a Multidisciplinary Test-Chain, J. Build. Eng. 69 (2023) doi:10.1016/j.jobe.2023.106251.
[50] International Organization for Standardization UNI EN ISO 7726 - Ergonomics of the Thermal Environment – Instruments for Measuring Physical Quantities; 2002.
[51] G. Salvalai, M.M. Sesana, Experimental Analysis of Different Insulated FaÇade Technologies in Summer Condition, J. Green Build. 14 (2019) 77–91, https://doi.org/10.3992/1943-4618.14.4.77.
[52] H. López-Moreno, A. Rodríguez-Sánchez, C. Viñas-Arrebola, C. Porras-Amores, Thermal Behavior of a Ventilated Façade using Perforated Ceramic Bricks, Int. J. Civ. Environ. Eng. 9 (2015) 905–910, https://doi.org/10.5281/zenodo.1109155.